IUPAC Technical Report

Helge Lemmetyinen, Nikolai V. Tkachenko, Bernard Valeur, Jun-ichi Hotta, Marcel Ameloot, Nikolaus P. Ernsting, Thomas Gustavsson and Noël Boens

Time-resolved fluorescence methods (IUPAC Technical Report)

Abstract: This IUPAC Technical Report describes and compares the currently applied methods for measuring and analyzing time-resolved fluorescence traces using phase-modulation fluorometry as well as pulse fluorometry (direct emission decay measurements, single-photon timing, streak camera measurements, fluorescence upconversion, and optical Kerr gating). The paper starts with a brief description of the basic principles for time and frequency domain fluorescence spectroscopy. The fundamental equations are given, and recommendations for adequate use are emphasized. The up-to-date, commonly employed excitation sources and photodetectors are described in detail. The analysis of time-resolved fluorescence data is discussed. Attention is paid to possible artifacts, and remedies are presented on how to avoid them or to account for them. Finally, fluorescence lifetime standards for the nanosecond and picosecond timescales are collected.

Keywords: fluorescence spectroscopy; IUPAC Analytical Chemistry Division; IUPAC Organic and Biomolecular Chemistry Division; IUPAC Physical and Biophysical Chemistry Division; phase-modulation fluorometry; pulse fluorometry; time-resolved fluorescence.

DOI 10.1515/pac-2013-0912
Received September 12, 2013; accepted May 30, 2014

CONTENTS

Article note: Sponsoring bodies: IUPAC Physical and Biophysical Chemistry Division; IUPAC Organic and Biomolecular Chemistry Division; IUPAC Analytical Chemistry Division; see more details on p. 1996.

Helge Lemmetyinen and Nikolai V. Tkachenko: Department of Chemistry and Bioengineering, Tampere University of Technology, P.O. Box 541, FI-33101 Tampere, Finland, e-mail: helge.lemmetyinen@tut.fi and nikolai.tkachenko@tut.fi
Bernard Valeur: Département CASER, Conservatoire National des Arts et Métiers, 292 rue Saint-Martin, 75003 Paris, France and Laboratoire PPSM, Ecole Normale Supérieure de Cachan, 61 Avenue du Président Wilson, 94235 Cachan, France, e-mail: bernard.valeur@cnam.fr
Jun-ichi Hotta: Graduate School of Science and Engineering, Yamagata University, 4-3-16 Jonan, Yonezawa 992-8510, Japan, e-mail: hotta@yz.yamagata-u.ac.jp
Marcel Ameloot: Hasselt University, Martelarenlaan 42, 3500 Hasselt, Belgium, e-mail: marcel.ameloot@uhasselt.be
Nikolaus P. Ernsting: Department of Chemistry, Humboldt-Universität zu Berlin, D-12489 Berlin, Germany, e-mail: nernst@chemie.hu-berlin.de
Thomas Gustavsson: CNRS, IRAMIS, LIDYL, Laboratoire Francis Perrin, URA 2453, 91191 Gif-sur-Yvette, France, e-mail: thomas.gustavsson@cea.fr
Noël Boens: Department of Chemistry, Katholieke Universiteit Leuven, Celestijnenlaan 200f – bus 02404, 3001 Leuven, Belgium, e-mail: Noel.Boens@chem.kuleuven.be

1 Basic principles

1.1 Introduction

Fluorescence spectroscopy and imaging have become indispensable tools for the non-invasive study of matter or living systems at a molecular or supramolecular level [1–3]. Indeed, fluorescence is a powerful method for investigating with high spatiotemporal resolution the structure and dynamics of organic and inorganic materials, biopolymers, cofactors, biological cells, and tissues in ensembles and at the single-molecule level. To study the time course (kinetics/dynamics) of excited states, the fluorescent sample is excited by modulated light at high frequency (phase-modulation fluorometry, Section 2) or by a short pulse of light (pulse fluorom-

etry, Section 3), and the resulting time-resolved fluorescence response is monitored. An in-depth discussion and comparison of the various techniques available for measuring time-resolved fluorescence – which differ in principle, excitation source, time resolution, photodetector, etc. – are the topics of this IUPAC Technical Report.

Time-resolved fluorescence techniques are commonly employed to determine the parameters characterizing the *δ-pulse response function* of a fluorescent sample (i.e., the temporal fluorescence response to an infinitely short pulse of light expressed mathematically as the Dirac delta function). *Phase-modulation fluorometry* uses modulated light at variable frequency and provides the harmonic response of the sample, which is the Fourier transform of the δ-pulse response. *Pulse fluorometry* uses a short excitation light pulse to give the δ-pulse response function of the sample, convoluted by the instrument response function. The first technique works in the frequency domain, the second in the time domain.

In the frequency domain, the phase and modulation measurements can be done by using either a continuous wave (cw) laser (or a xenon lamp) and an optical modulator, or the harmonic content of a pulsed laser.

In time domain, the most widely used technique is *time-correlated single-photon counting* (TCSPC), preferably called *single-photon timing* (SPT) according to the recommendations of the IUPAC Subcommittee on Photochemistry [4]. *Time gated* systems are less popular. *Streak cameras* offer a very good time resolution (a few ps or less). The instruments that provide the best time resolution (tens of femtoseconds) are based on *fluorescence upconversion*. *Optical Kerr gating* also provides excellent time resolution.

The principles of these techniques will be briefly presented and compared, and recommendations for adequate use will be emphasized. For more details, the reader is referred to the relevant books, book chapters, and reviews [1–3, 5–7]. Attention will be paid to possible artifacts. A list of lifetime standards is also given. Time-resolved fluorescence anisotropy measurements will not be discussed here, because they are described in a separate IUPAC Technical Report [8].

1.2 Basic equations

The *δ-pulse response function* $i(t)$ of a fluorescent sample is, in the simplest case, a single exponential:

$$i(t) = \alpha\, e^{-t/\tau} \tag{1}$$

where t denotes time, τ represents the (excited-state) *lifetime*[1] and α is a scaling factor. $i(t)$ of a fluorescent sample is the temporal fluorescence response to an infinitely short pulse of light, that is, the fluorescence decay one would theoretically observe after an excitation pulse of infinitely short duration described by the Dirac δ-function.

More frequently, $i(t)$ is a sum of discrete exponentials (eq. 2) or a more complicated function; sometimes, the system is characterized by a distribution of *decay times*.[1]

$$i(t) = \sum_i \alpha_i\, e^{-t/\tau_i} \tag{2}$$

In eq. 2, τ_i stands for the *i*th *decay time*[1] and α_i is its associated pre-exponential factor. For any experimental excitation function $E(t)$, the measured fluorescence response $R(t)$ of the sample is the convolution of $E(t)$ and the fluorescence δ-pulse response function $i(t)$:

$$R(t) = E(t) \otimes i(t) = \int_0^t E(s)\, i(t-s)\, \mathrm{d}s \tag{3}$$

1 The term *lifetime* τ of a molecular entity in the excited state is reserved exclusively for an entity which decays mono-exponentially. *Lifetime* has the meaning of the average time a molecular entity remains in the excited state before de-excitation. Whenever this physical meaning is not valid, the term *lifetime* is not correct, and the general-purpose expression *decay time(s)* should be employed. For instance, each component e^{-t/τ_i} of $i(t)$ in eq. 2 represents an exponentially decaying function (because $t > 0$ and $\tau_i > 0$), and hence τ_i represents a *decay time*. A rise of $i(t)$ (eq. 2) is possible due to the presence of a negative pre-exponential α_i in combination with an exponentially decaying function e^{-t/τ_i}. The decay times τ_i in a multi-exponential decay (eq. 2) are lifetimes only if they can be linked to specific molecular entities in the excited state, which each decay as a single exponential (e.g., a collection of mono-exponentially decaying fluorophores). Conversely, a lifetime is always a decay time.

where ⊗ denotes the convolution operator, and t and s represent time. Equation 3 does not refer to any particular measurement technique and can be used to calculate the output signal $R(t)$ of any instrument with known excitation function $E(t)$ for any δ-pulse response function $i(t)$.

In phase-modulation fluorometry, the sample is excited by light which is sinusoidally modulated at high frequency with modulation depth m_0 (AC/DC ratio). The fluorescence response, which is the convolution (eq. 3) of the δ-pulse response function and the sinusoidal excitation function, is sinusoidally modulated at the same frequency but delayed in phase and partially demodulated with respect to the excitation. The phase shift ϕ and the modulation ratio $M = m/m_0$, where m is the modulation depth of the fluorescence, characterize the harmonic response of the system. These parameters are measured as a function of the modulation frequency (Fig. 1).

It should be noted that the harmonic response is the Fourier transform of the δ-pulse response, as expressed by the following relation [1]:

$$M(\omega)\, e^{-j\phi(\omega)} = \int_0^\infty i(t)\, e^{-j\omega t}\mathrm{d}t \tag{4}$$

where ω is the angular frequency ($\omega = 2\pi f$) and $i(t)$ is the δ-pulse response normalized according to $\int_0^\infty i(t)\,\mathrm{d}t = 1$.

Consequently, the following useful relations are obtained [1]:

$$\phi = \tan^{-1}\left(\frac{P}{Q}\right) \tag{5}$$

and

$$M = (P^2 + Q^2)^{1/2} \tag{6}$$

where P and Q are the sine and cosine transforms of the δ-pulse response, respectively.

In the case of a single exponential decay, the lifetime can be determined either by phase measurements

$$\tau_\phi = \frac{1}{\omega}\tan\phi \tag{7}$$

or modulation measurements

$$\tau_M = \frac{1}{\omega}\left(\frac{1}{M^2} - 1\right)^{1/2} \tag{8}$$

Phase-modulation fluorometry is discussed in Section 2, and details about data analysis are presented in Section 4.

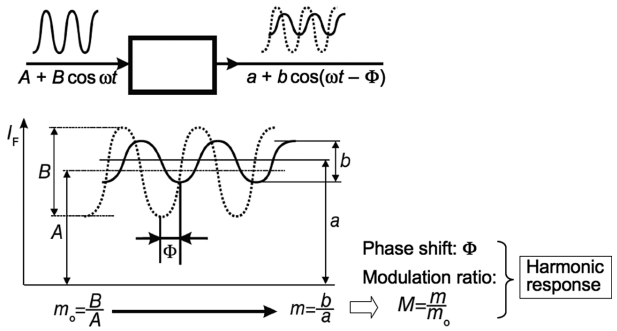

Fig. 1 Principles of phase-modulation fluorometry. Adapted from ref. [1].

In pulse fluorometry, the sample is excited by a short light pulse $E(t)$ and the fluorescence response $R(t)$, expressed by eq. 3, is recorded as a function of time t. When the excitation light pulse $E(t)$ is infinitely short (mathematically described by the Dirac delta function), then eq. 3 reduces to $R(t) = i(t)$; otherwise, the convolution integral of eq. 3 describes $R(t)$. Pulse fluorometry is discussed in Section 3, and details about data analysis are given in Section 4.

2 Phase-modulation fluorometry

2.1 General considerations

The two lifetime values calculated according to eqs. 7 and 8 should of course be identical and independent of the modulation frequency. This allows one to check whether an instrument is correctly tuned by using a lifetime standard whose fluorescence decay is known to be mono-exponential. Note that a significant difference between values obtained by means of the above equations is compelling evidence of non-exponential behaviour of the fluorescence decay.

In principle, the theory shows that a single frequency ω suffices for measuring the lifetime τ of a single exponential decay but the frequency should be chosen such that $\omega\tau$ is not too different from unity, i.e., $f \approx 1/(2\pi\tau)$. Therefore, for lifetimes of 10 ps, 1 ns, and 100 ns, the optimum frequencies are about 16 GHz, 160 MHz, and 1.6 MHz, respectively.

In practice, multi-frequency instruments are currently used. They are based on both continuous and pulsed excitation light sources as described in Sections 2.2 and 2.3. Each type of excitation source sets particular requirements to detectors and electronics.

2.2 Phase fluorometers using a continuous light source and an electro-optic modulator

The light source can be a xenon lamp in combination with a monochromator. The optical configuration should be carefully optimized because the electro-optic modulator (usually a Pockels cell, PC) has a small acceptance angle. The modulation frequency typically ranges from 0.1 to 300 MHz. The advantages are the low cost of the system and the broad range of excitation wavelengths [9].

In terms of light intensity and modulation, it is preferable to use a cw laser whose cost is reasonable. Readily available conventional lasers and wavelengths are the following: He–Cd: 325, 442.5 nm; He–Ne: 543.3, 594.1, 611.9, 632.8 nm; Ar: 457.9, 476.5, 488, 514.5 nm. Nowadays, several types of semiconductor emitting diodes and lasers with wavelengths covering most of the visible (vis) spectral region can also be used. Essentially, such semiconductor diode lasers may be preferable for this application because the light modulation is much easier.

Figure 2 shows the schematic diagram of a multi-frequency phase-modulation fluorometer. A beam splitter reflects a few percent of the incident light towards a reference photomultiplier tube (PMT) (via a cuvette containing a scattering suspension or not). The fluorescent sample, S, and a reference, R (containing either a scatterer or a fluorescent compound), are placed in a rotating turret. The emitted fluorescence or scattered light is detected by a PMT through a monochromator or an optical filter. The Pockels cell (PC) is driven by a frequency synthesizer, and the PMT response is modulated by varying the voltage at the second dynode by means of another frequency synthesizer locked in phase with the first one. The two synthesizers provide modulated signals that differ in frequency by a few tens of Hz in order to achieve cross-correlation. This procedure offers an excellent accuracy because the phase and modulation information contained in the signal is transposed to the low-frequency domain where phase shifts and modulation depths can be measured with a much better accuracy than in the high-frequency domain. For instruments using a cw laser, the standard

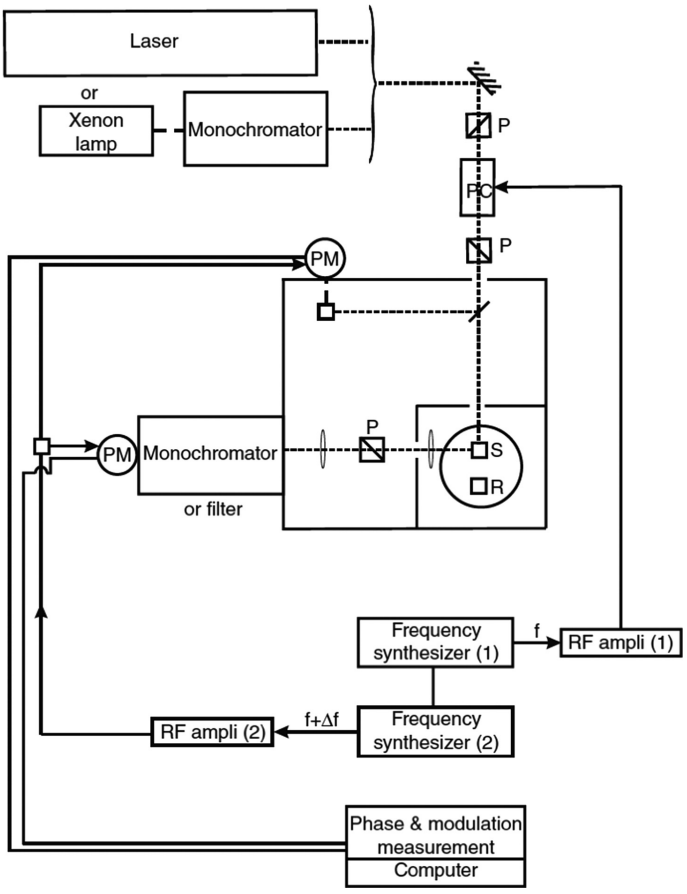

Fig. 2 Schematic diagram of a multi-frequency phase-modulation fluorometer. P: polarizers, PC: Pockels cell, PM: photomultiplier (tube), R: reference, RF ampli: radiofrequency amplifier, S: sample. The phase shifts and the modulation depths are measured by an electronic device, and their values are processed by a computer. Reprinted with permission from ref. [1].

deviations are currently (0.1–0.2)° for the phase shift and 0.002–0.004 for the modulation ratio. When the light source is a xenon lamp, these standard deviations are ca. 0.5° and 0.005, respectively.

Practically, the phase delay ϕ_R and the modulation ratio m_R of the light scattered by a solution of glycogen or a suspension of colloidal silica used as reference are measured with respect to the signal detected by the reference PMT. Then, after rotation of the turret, the phase delay ϕ_F and the modulation ratio m_F for the sample fluorescence are measured with respect to the signal detected by the reference photomultiplier. The absolute phase shift and modulation ratio of the sample are then $\phi = \phi_F - \phi_R$ and $M = m_F/m_R$, respectively.

2.3 Phase fluorometers using the harmonic content of a pulsed laser

A laser system that delivers pulses in the ps range with a repetition rate of a few MHz can be considered as an intrinsically modulated source. The harmonic content of the pulse train – which depends on the width of the pulses – extends to several GHz [10]. The limitation is due to the detector. For high-frequency measurements, it is absolutely necessary to use microchannel plate PMTs (because they have a much faster response than common PMTs). The highest available frequencies are thus close to 2 GHz [11].

Ti:sapphire lasers are most suitable for both pulse and phase fluorometers: decay times as short as 10–20 ps can be measured. It should be noted that internal cross-correlation is not possible with microchannel plate PMTs, but an external mixing circuit can be used.

3 Pulse fluorometry

3.1 Up-to-date excitation sources and detectors

In this section we will focus on recent developments in the areas of excitation sources and detectors that lead to a good overall system performance. The choice of the components in the measurement system is crucially important for performing reliable measurements.

3.1.1 Excitation sources

A fundamental component in time-resolved fluorometry is the pulsed light source. In general, excitation sources can be divided into coherent light sources like lasers and incoherent light-emitting diodes (LEDs).

One of the most popular excitation sources in time-resolved spectroscopy is the Ti:sapphire laser. These laser systems use diode-pumped solid-state cw lasers as pump source for Ti:sapphire oscillators and feature self-alignment and computer-controlled tuning. Ti:sapphire laser systems deliver pulses in the 690–1020 nm tuning range with pulse duration from 20 fs to a few ps. The spectral range can be extended in the visible by using frequency conversion and/or optical parametric oscillators (OPOs) or optical parametric amplifiers (OPAs). Current, commercially available systems have a tuning range of 680–1300 nm, which can be complemented with a second harmonic generator to cover the visible and near UV parts of the spectrum (340–650 nm). The repetition rate of these laser systems can be adjusted by means of a pulse picker or via a regenerative amplifier in case such a system is used.

Pulsed diode lasers are one of the most frequently used light sources in the field of time-resolved photoluminescence. These reliable and easy-to-use excitation sources can generate pulses with a repetition rate up to 80 MHz and a width down to 50 ps. One interesting feature is the ability to tune the repetition rate freely without a pulse picker or a PC. Moreover, pulsed diode lasers are available with different excitation wavelengths, covering a broad spectral range from 375 nm to near infrared (NIR). There are also specially designed modules delivering excitation at 266 nm by means of harmonic generation.

The fibre laser consists basically of a diode laser and a doped fibre of a fixed length. This laser delivers pulses with a width from 100 fs to a few ps in the 1060–1600 nm wavelength range with a fixed repetition rate of typically several tens of MHz to more than 100 MHz. The main drawback of this robust excitation source is its rather inflexible optical setup. However, the repetition rate of this laser can be adjusted by means of a pulse picker. The wavelength of the pulsed fibre laser can be frequency doubled or tripled. Recently, the super continuum laser, where a photonic crystal fibre is excited by a fibre laser to generate white laser light, is starting to be used as a convenient excitation source. The super continuum laser has a wide wavelength range (390–2400 nm), and the desired wavelength can be selected by using appropriate optical filters. The pulse duration varies depending on the system and bandwidth of the selected wavelength, typically from a few tens of ps to a few hundreds of ps [12].

Pulsed LEDs are interesting excitation sources in time-resolved spectroscopy because they can fill in the gaps in the spectral range not covered by the diode lasers. Even LEDs with wavelengths down to 240 nm are now available [13]. These LEDs can be pulsed up to 10 MHz at pulse widths down to 500 ps. Although this is a broad pulse width compared to pulses from laser excitation sources, it is much smaller than the decay times of many fluorophores.

3.1.2 Detectors

The choice of the photodetector depends on the type of signal detection used, direct recording of the transient signal, timing measurements (single-photon timing), or time-independent signal integration (optical correla-

tion methods such as fluorescence upconversion or optical Kerr gating). The criteria for choosing the detector are widely different according to the cases, as outlined below.

For a long time the only photodetectors used for the measurement of emission decay curves were PMTs. PMTs can be used in two modes, intensity and photon counting, but not all PMTs allow the photon counting mode. There are also gated PMTs. The gate mode can be used to reduce effects of overshoot signal due to scattered light, for example.

In the direct emission decay measurement, transient emission intensity after excitation is detected with PMTs with a fast response. The response of PMTs needs to be reasonably fast compared to the overall decay of the emission intensity. The output from PMTs is proportional to the intensity of the fluorescence at each moment. Therefore, one can instantly obtain emission decay curves by recording the output from PMTs with adequate devices, like digital storage oscilloscopes. Detailed requirement for direct emission intensity measurements is discussed in Section 3.2.

In photon counting mode, the output signal of a PMT is a series of short pulses each of which corresponds to a detected photon. These pulses are usually passed to a discriminator, an electronic device converting pulses with amplitude greater than a preset threshold value to pulses with constant amplitude and rejecting the pulses that are lower in amplitude than the threshold value. The role of the discriminator is to distinguish between the pulses produced by the photons and by thermal electrons. Thus, an electric pulse is observed as the output of the PMT–discriminator combination for each detected photon.

Generally, the ability of a PMT to operate in photon counting mode depends on its dark count rate (which is analogous to dark current in intensity measuring mode). The main factors determining the dark count rate are the type of the photocathode and the temperature of the photocathode. Typically, cathodes with higher work function provide lower dark count rates. This is due to the lower probability to emit a thermal electron at higher work function, and this is the reason for PMTs with lower red wavelength threshold for exhibiting a high dark count rate. The probability to emit a thermoelectron increases with the temperature. Therefore, the dark count rate can be reduced by cooling down the photocathode, which is the usual measure to achieve a reasonably low dark count rate for PMTs with sensitivity range extended to the red and NIR part of the spectrum. A dark count rate for carefully designed PMTs with sensitivity range in UV–vis range can be as low as a few counts/s at room temperature.

The maximum photon counting rate depends on the pulse response time of the PMTs and the recovery time of the discriminator, called dead-time (the shorter the dead-time, the higher the counting rate can be). If photons are arriving with too short a delay between them, the detector will have no time to respond and the output will be a single pulse (probably with longer duration). This type of malfunctioning results in an inaccuracy in measurements called *pile-up distortion*. For high-performance devices, the maximum counting rate can be 10–40 MHz. If the desired accuracy of measurements is δ and the detector dead time is Δt, then the maximum counting rate must be lower than $f = 2\delta/\Delta t$ [14]. The value provided in detector specifications as "maximum count rate" refers usually, but not always, to the maximum frequency which may appear on the device output, but the probability to count two photons as one may be unreasonably high in this case.

Several types of avalanche photodiodes (APDs) have been developed which can operate in photon counting mode. Typically these devices have a small photosensitive area (the smaller the area, the lower the dark current and the shorter the response time are) and have found applications in instruments working with small emitting objects, e.g., in microscopy applications.

Photon counting is widely used in all applications dealing with low light intensities. Steady-state fluorometers can utilize photon counting techniques to achieve the highest sensitivity. In time-resolved measurements, photon counting has a special application called single-photon timing (or time-correlated single-photon counting). It is one of the most important techniques used in time-resolved spectroscopy and will be considered separately in Section 3.3.

Photon counting is widely used in upconversion emission decay measurements where a low-intensity beam at sum frequency must be measured (Section 3.5). For the upconversion method, the time steps for decay measurements are determined by the relative delay between the fluorescence and gate pulse (delay

obtained via spatial displacement of the optical delay line), and can be as short as a few fs, although the time resolution is generally determined by the width of the light pulses used.

Development of new devices and techniques made it possible to come within reach of photon counting sensitivity in many spectroscopy applications. For example, light intensifiers based on microchannel plate PMTs in combination with streak cameras and high-sensitivity CCD detectors are used in commercial systems giving 2 ps time resolution and photon counting sensitivity at the same time (Section 3.4).

3.2 Direct emission decay measurements (>100 ps)

A typical scheme for the direct measurements of photoinduced emission time profiles is presented in Fig. 3.

The sample is excited by a short light flash. Nowadays, the excitation pulse sources are typically ns pulsed lasers. Photoluminescence is collected by a lens or a mirror and directed to a monochromator to select the observation wavelength of interest. The signal from the photodetector at the monochromator output is recorded by, e.g., a digital oscilloscope. To improve the signal-to-noise ratio, the measurements can be repeated a few times, accumulating (summing up or averaging) the signal in a computer or oscilloscope memory. However, the method allows a single-shot measurement, which is important for samples with strong photodegradation.

The time-resolved fluorescence should actually be viewed as a 2D data surface, which in principle can be sampled either along the time or the wavelength axis. Time-resolved emission spectra can be measured directly using polychromatic detection, or can be reconstructed from kinetic traces. In the latter case, the fluorescence time responses $R(t, \lambda_{em})$ at a series of wavelengths λ_{em} are measured independently. Before proceeding, data must be corrected by applying a spectrum correction procedure. Basically, the time integral of each kinetic trace for a given wavelength is scaled with regards to the corresponding intensity $R^{SS}(\lambda_{em})$ in the steady-state fluorescence spectrum:

$$\int_0^\infty R(t, \lambda_{em})\, dt = R^{SS}(\lambda_{em}) \tag{9}$$

Plotting the dependence of the corrected signal intensities for a given delay time as a function of the wavelength λ_{em} yields the corrected time-resolved emission spectrum at a certain delay. Maroncelli and Fleming have described this spectral reconstruction method in detail [15].

If time-resolved spectra are the primary objective of the measurements, a gated CCD detector can be used as photodetector. Then the recorded signal is the uncorrected spectrum in the time interval determined by the gating system, which has to be corrected for the spectral sensitivity of the detector. Naturally, the measurements can be repeated at a series of delays to track the decay profiles as well.

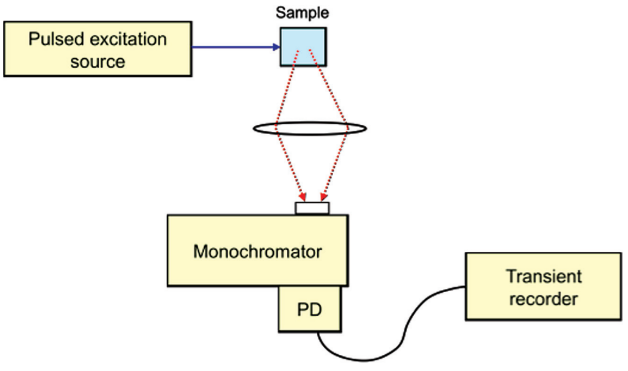

Fig. 3 Scheme of direct emission decay measurements. PD denotes a photodetector.

The choice of the photodetector depends on the detection wavelength range, time resolution, and signal intensity. For measurements in the UV–vis spectral range, PMTs and gated PMTs are widely used. Typical cut-off wavelength for bi-alkali photocathodes is 650 nm, and for multi-alkali is 850–900 nm. For measurements in the vis–NIR range, Si photodiodes can be used. A typical sensitivity range for Si photodiodes is 400–1100 nm. There are also PMTs with sensitivity extended up to 1100 nm (e.g., equipped with S-1 type photocathodes). These PMTs have relatively high dark current, which can be reduced gradually by cooling down the photocathode (typical operational temperature is –40 °C). To extend the detection range further to the IR, Ge and InGaAs photodiodes are employed whose sensitivity range ranges from 900 to 1700 nm. Avalanche photodiodes are also finding applications in these instruments because they provide higher sensitivity as compared to traditional diodes, and can outperform PMTs at relatively high photon flux. A common requirement for photodetectors is high linearity and low dynamic distortions of the response, i.e., of photocurrent or photovoltage generated by the detector.

For high time resolution applications, the excitation sources are typically pulsed lasers. These can be laser systems based on Nd:YAG Q-switched lasers or excimer lasers used directly or pumping dye or Ti:sapphire tuneable lasers. Recently, optical parametric generators were designed, which provide a wide tuning range and sufficient pulse energy to be used as excitation sources. For this kind of laser system, the pulse width is 5–20 ns and the excitation wavelength can be from UV to NIR with pulse energy varying from a few mJ to J.

Typical applications of the method are measurements of the emission decays in the ns to s time domain. For example, emission of metal ions in glass matrices or phosphorescence of organic dyes can be observed in the μs to ms timescale. Time-resolved measurements of phosphorescence do not require a high time resolution but demand a high sensitivity of the detection system because the efficiency of the phosphorescence is usually rather low due to numerous quenching mechanisms. Cooled PMTs are used for measurements in the vis and NIR ranges.

In comparison to single-photon timing (Section 3.3), if both methods are applicable, the advantage of the direct measurements is the possibility to obtain the decay curve from a single excitation flash. A disadvantage is the lower accuracy of the measurements. Nonlinear distortions of the signal by the detector and transient recorder sum up and increase the total measurement inaccuracy, whereas the photon counting nature of the single-photon timing method allows one to avoid these types of inaccuracies and to obtain a high dynamic range.

Extending the time resolution to sub-nanosecond timescale with direct light intensity measurement by traditional methods faces at least two problems. First, one has to use pulsed excitation light sources with a short pulse duration (a few ps) and relatively high pulse energy (at mJ level). Such lasers are rather expensive and complex systems. Second and most importantly, the time resolution approaches the limits of modern electronics, detectors, and recording systems. For example, the typical time resolution of PMT detectors is close to 1 ns and limited by the dispersion time of the electrons in a dynode chain. A better time resolution (0.1 ns and faster) can be achieved from *p-i-n* photodiode detectors at the expense of the size of the sensitive area and requiring high-bandwidth state-of-art amplifiers. General purpose transient recorders have response times ranging down to 0.5 ns. There are devices with a few times better resolution at a considerable price increase.

3.3 Single-photon timing (SPT) (few ps to few 100 μs)

The most widely used technique developed specifically for time-resolved fluorescence measurements on the sub-nanosecond timescale is single-photon timing, SPT (alternatively known as time-correlated single-photon counting, TCSPC) [5, 7, 16]. It is characterized by extremely high sensitivity (even a single molecule can be studied) and provides time resolution down to a few ps. Moreover, it is a relatively inexpensive method and various versatile commercial instruments are available.

The basic principle of the method relies on the fact that the probability of detecting a single photon at time *t* after an exciting pulse is proportional to the fluorescence intensity at that time. After timing and

recording the single photons following a large number of excitation pulses, a fluorescence decay histogram is reconstructed. In a typical experiment, the sample is excited by a short laser pulse, with a well-defined polarization. A small part of the excitation light is split off and detected by a fast photodiode to serve as the triggering pulse. The emission from the sample is collected at right angle, passed through a polarizer to a monochromator, and detected by a photomultiplier working in photon counting mode. The electric pulses from the photodiode and the photomultiplier are each directed to a constant fraction discriminator (CFD), which improves the timing characteristics of the signals. These signals are then passed to a time-to-amplitude converter (TAC), which is a pulse-controlled generator of a linearly rising voltage signal. The pulse from the photodiode (START) starts the generator operation and the pulse from the PMT (STOP) stops it. Thus, the output voltage U of the TAC is determined by the delay time, Δt, between the laser pulse and the first detected emission photon, i.e., $U \propto \Delta t$. The output voltage of the TAC is analyzed by a multichannel analyzer (MCA) equipped with a memory divided into N channels. Each channel is associated with a discrete voltage value generated by the TAC. Each start–stop sequence increments a given channel in the MCA with one event. By repeating the start–stop sequence many times, a histogram is obtained, describing the probability distribution of photon emission at a given wavelength.

In order to compensate for the PMT dead time, it is important to keep the detection rate so low that the probability for a second photon arriving during the same start–stop sequence is close to zero. In practice, this means that the maximum detection rate of fluorescence photons must be kept much smaller than the number of exciting pulses (<0.01–0.05 detected pulses per exciting pulse). When using high-repetition-rate lasers, working at a few tens of MHz, the maximum fluorescence photon count rate should thus be a few tens of thousands of counts/s. This means that for most START pulses, no STOP photons arrive. In order to assure that the TAC is properly recharged at the beginning of each start–stop sequence, it is advantageous to work in the INVERSE mode, using the PMT signal as START and the photodiode signal as STOP. The histogram is then simply inverted to obtain the correct time profile. Sometimes it is necessary to reduce the repetition rate of the laser (e.g., by a pulse picker) to ensure that the time distance between two consecutive laser pulses is at least 10 times the decay time to avoid distortion of the measured decay.

Historically, a SPT setup was built from discrete analogue electronics units (CFD, TAC, MCA). Today, a full SPT configuration is found on a plug-in PC board, coming with the software needed for setting the parameters and running the experiment.

Figure 4 shows a schematic overview of a typical single-photon timing setup using a modern plug-in SPT board mounted in a PC.

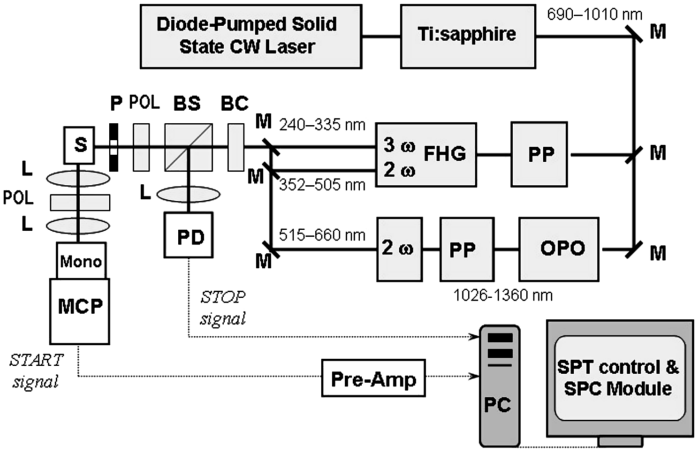

Fig. 4 Schematic overview of a modern single-photon timing setup. BC: Berek compensator, BS: non-polarizing beam splitter, FHG: frequency harmonic generator, L: lens, M: mirror, MCP: microchannel plate, PMT: photomultiplier tube, Mono: monochromator, OPO: optical parametric oscillator, P: pinhole, PC: personal computer, PD: photodiode, POL: polarizer, PP: pulse picker, Pre-Amp: preamplifier, S: sample (compartment), SPT module: contains constant fraction discriminator (CFD), time-to-amplitude converter (TAC), and multichannel analyzer (MCA). The available usable wavelengths are also indicated.

3.4 Streak camera (1 ps to 10 ns)

A special type of electron tubes, which are called streak cameras, was developed to measure short light pulses. Originally the aim was to measure single but powerful light pulses (typically generated by pulsed lasers). In single short measurements, the time resolution of modern streak cameras can be better than 1 ps. Also, there are streak cameras developed for fast emission decay measurements, which can detect rather low light intensity and operate also in repetition mode.

3.4.1 Principles

The streak camera is an electronic device that converts the temporal light intensity dependence to a spatial distribution of electrons or secondary photons. A schematic presentation of its operational principles is shown in Fig. 5. The incoming photon flow (the signal to be recorded) is converted to photoelectrons by a photocathode. The photoelectrons are accelerated by an electric field and passed to a deflection system, which is supplied by a high-speed sweep voltage to deflect the electron beam across a phosphor screen. The swept electron beam produces an emitting trace on the screen, which can be read out, e.g., by a CCD detector. In this way the temporal dependence is converted into the spatial dependence along the sweeping axis.

Additionally, the incoming light can be spread spectrally in the direction perpendicular to the sweeping direction at the photocathode. Then, the 2D image on the streak camera output screen presents the time-wavelength data array. This allows one to reconstruct both time and spectrum emission evolution at a single excitation pulse.

3.4.2 Method

Characteristics. The spectral range of a streak camera is determined by the type of photocathode (e.g., S-20 photocathode sensitivity range is roughly 200–850 nm). Naturally, the spectrum sensitivity correction procedure must be applied to measure true time-resolved emission spectra.

The typical time resolution of streak cameras designed for spectroscopy applications is a few tens of ps. For the fastest instruments, the time resolution can be as short as 200 fs. However, such a high time resolution is only achieved in single-shot mode, and thus requires a strong light intensity on the device input. In repetition mode, the time resolution is limited by trigger jitter of the control electronics and reduces time resolution to >10 ps. In this respect, the time resolution benefits of the method are best available for samples with high emission efficiency, when the single-shot experiment provides reasonable signal intensity.

It is technically difficult to provide constant velocity of the electron beam sweeping the screen. Therefore, sweep and intensity correction procedures are applied to the data read-out from the screen to obtain true emission time profiles. The time and wavelength correction routines are usually included in the software package supplied with the instrument.

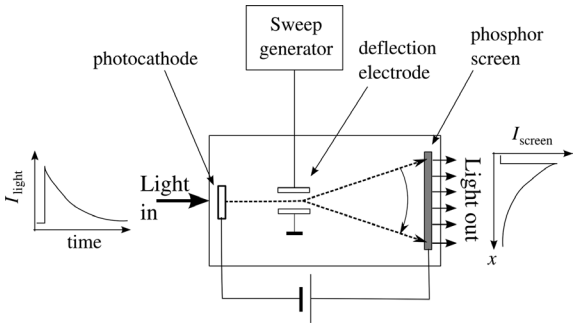

Fig. 5 Time-resolved measurements using a streak camera.

Comparison with other methods. The most distinct advantage of streak cameras is their ability to obtain both temporal and spectral information of the emission in one shot. This unique property of the method is not available from any other current method in fast and ultrafast timescales.

In terms of time resolution, the streak cameras take an intermediate position between single-photon timing (time resolution ≈ 10 ps) and frequency upconversion methods (capable of reaching a time resolution better than 100 fs). In emission spectroscopy applications, streak cameras are typically used in the time domain from 10 ps to μs.

The sensitivity of streak cameras can be improved by adding a microchannel plate amplifier in front of the phosphor screen, so that the electron flow is amplified before hitting the screen (e.g., Streakscope C4334, Hamamatsu Co.). These devices approach single-photon timing in terms of sensitivity, although the price of such systems remains rather high. Therefore, typical applications of streak cameras are limited to samples with relatively high emission intensities, whereas single-photon timing can also be used when very low intensities have to be measured, e.g., in single-molecule spectroscopy.

3.5 Fluorescence upconversion (tens of fs to 1 ns)

3.5.1 Introduction

Fluorescence upconversion allows recording of fluorescence with very high time resolution, basically limited by the temporal width of the laser pulses being used. For example, using a home-built cavity-dumped Ti:sapphire laser producing ultra-short pulses, a time resolution of about 40 fs has been reported [17]. The present text is intended for non-specialists wishing to design an experiment. It should be remarked that commercial setups, excluding the laser, working in the vis spectral region are available [18].

Fluorescence upconversion is a variant of sum-frequency generation [19], which in turn is a generalization of second harmonic generation; it is also closely related to parametric amplification [20, 21]. Basically, an intense gate pulse at frequency ν_G (Fig. 6) is mixed with the fluorescence at frequency ν_F in a nonlinear optical crystal, to create a short pulse at the sum frequency $\nu_U = \nu_G + \nu_F$. The gate pulse thus represents a time window for the fluorescence during which the fluorescence is upconverted, and the intensity of the upconverted light is directly proportional to the fluorescence intensity during this time window. By controlling the optical delay between the fluorescence and the gating pulse, kinetic traces of the fluorescence can be obtained. Because the upconverted signal appears far to the blue of the fluorescence band, a monochromator or an optical filter easily separates it from both fluorescence and laser emission. As a result, one of the main advantages of this technique is that the upconverted signal recorded is nearly background free. Another aspect of the upconversion technique is that near- to mid-infrared fluorescence in the 1–5 μm spectral region can be measured in

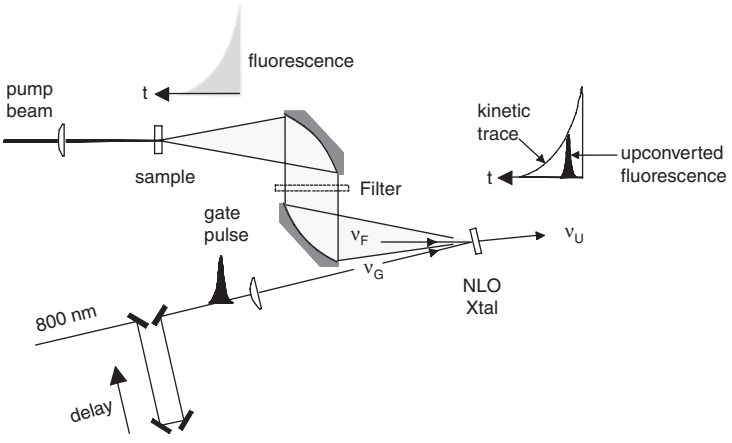

Fig. 6 Typical setup for fluorescence upconversion. NLO Xtal represents a nonlinear optical crystal.

the vis spectral region after upconversion. This constitutes a great advantage with regards to the choice of the detector.

The first physicochemical study with this technique was reported by Mahr and Hirsch in 1975 [22]. Since then the number of articles using this technique increases steadily every year.

3.5.2 Instrumental schemes

Laser and detection. The choice for a fluorescence upconversion setup depends foremost on the required excitation wavelengths. The optimal detection method is then largely determined.

When excitation can stay limited to the second or third harmonic (denoted SH and TH, respectively) of a fundamental laser system, a fs oscillator will suffice [18, 23]. For instance, a modern mode-locked Ti:sapphire oscillator typically delivers pulses at 800 nm, bandwidths of 60–10 nm corresponding to near transform-limited pulse widths from <25 fs to 100 fs with average optical power of >1.5 W and a repetition rate of 80 MHz. To generate pump pulses, either frequency-doubling (or second harmonic, SH: 500 mW, 6 nJ per pulse) or frequency-tripling (or third harmonic, TH: 50 mW, 0.6 nJ per pulse) is readily achieved with 1 mm BBO (Table 1) crystals. The SH or TH pump beam is separated from the residual fundamental beam and focused into the sample cell by a short focal-length ($f = 30$ mm) quartz lens. The fluorescence is collected by an off-axis parabolic mirror (typically $f = 100$ mm), transported as a parallel beam through a low-pass color filter to cut the excitation light (important in order to reduce background from pump scatter) and focused into the sum-frequency crystal by a second parabolic mirror, often identical to the first one. The remaining part of the fundamental beam (5 nJ per pulse) is passed through the optical delay line and focused into the sum-frequency crystal with a lens ($f \approx 100$ mm), serving as gating pulse. A displacement Δx of the delay line corresponds to a time delay $\Delta t = 2\Delta x/c$, where c is the velocity of light. For example, a displacement of 150 μm corresponds to a time delay of 1 ps. Today, high-precision, motorized delay stages with a step of 0.1 μm, corresponding to 0.67 fs, are readily available. It may be necessary to use an 800-nm half-wave plate to control the polarization of the gate pulses, depending on whether a type I or type II crystal is being used. An additional half-wave plate is needed for the excitation beam, in order to choose the excitation polarization either parallel or perpendicular to the detection polarization, thus allowing the determination of fluorescence anisotropy. The upconverted UV light is spatially separated from the gate and pump light, spectrally selected by a double monochromator, and detected by a PMT running in photon counting mode. Since the count rate should normally remain 3 orders of magnitude below the excitation repetition rate, count rates up to about 100 kHz are technically possible, but normal rates are about 1 kHz.

A continuous range of excitation wavelengths becomes available with regenerative amplified laser systems. The output pulses of the Ti-sapphire oscillator form the seed for a regenerative amplifier where the peak power can be increased to a few GW and the repetition rate is decreased to the kHz range (1–250 kHz).

Table 1 Properties of nonlinear optical crystals for fluorescence upconversion.

	d_{eff}	d_{eff}/(pm·V^{-1}) 800 + 600	η(rel)	I_d /(GW·cm^{-2})	λ_{min}/(nm)	$\lambda_{fluo,min}$/(nm)
KDP (ooe)	$d_{36}\ sin\theta\ sin2\varphi$	0.3440	1.0	30 (532 nm/30 ps)	240	343
LBO (ooe)	$d_{32}\ cos\theta$	0.6420	2.8	>80 (800 nm/1 ps)	261	388
BBO (ooe)	$d_{31}\ sin\theta - d_{22}\ cos\theta\ sin3\varphi$	1.9700	24.6	10 (694 nm/20 ps)	189	247
$LiIO_3$ (ooe)	$d_{31}\ sin\theta$	4.5300	77.0	12 (532 nm/32 ps)	300	481

d_{eff} denotes the effective nonlinear susceptibility, η is the quantum efficiency of conversion, and I_d the damage threshold. λ_{min} is the smallest sum-frequency wavelength as limited by the transmission of the crystal. $\lambda_{fluo,min}$ is the corresponding smallest fluorescence wavelength supposing the gate is at 800 nm. KDP, LBO, and BBO stand for potassium dihydrogen phosphate (KH_2PO_4), lithium triborate (LiB_3O_5), and beta barium borate (β-BaB_2O_4), respectively. The indices ooe correspond to the polarizations of the gate, the fluorescence and the upconverted light relative to the ordinary axis of the crystal. This equals type I phase matching.

This has the further advantage of allowing the molecular system to relax before another excitation event begins. In this case, the high-peak power fundamental pulses can be used to seed an optical parametric oscillator/amplifier (OPO/OPA), the output of which can be frequency-doubled and/or frequency-mixed to provide pump pulses nearly anywhere in the UV–vis–NIR range. Note that parametric generation of pump light becomes easier as the fundamental peak power is increased. But the price is a lower repetition rate, and as a consequence, photon counting becomes less efficient for the reasons given above. It follows that detection by photon counting favours laser repetition rates well above 10 kHz [24, 25]. For example, by using an OPA pumped by a regenerative amplifier at a repetition rate of 250 kHz, excitation pulses centred at 490 nm with a pulse energy of ~5 nJ, a repetition rate of 250 kHz, and a temporal width of 50 fs were produced [26].

At lower repetition rates, photon counting is less efficient. Using a 1 kHz amplified Ti:sapphire laser system, Atas et al. built an upconversion setup for UV fluorescence [27]. Starting from 90 fs, 0.6 mJ pulses at 800 nm, they frequency tripled 80 % of the energy to 266 nm for excitation and used the remaining 20% for gating in a 0.2-mm type I BBO crystal. The resulting sum-frequency signal was filtered by a double monochromator and detected with a PMT. With lock-in techniques (heterodyne method), combined with boxcar integration, a signal-to-noise ratio of 50:1 can be achieved. Even at 1 kHz, the use of gated photon counting has been reported [28].

Choice of crystal. The crystals most often used for SH generation are $LiIO_3$, KDP, and especially BBO (Table 1). The characteristics of a great number of nonlinear optical crystals have been compiled by Dmitriev, Gurzadyan, and Nikogosyan [29]. The search for new crystals continues, in particular for use in the UV [30]. Various borate-containing crystals seem to be good candidates, but CLBO (caesium lithium borate, $CsLiB_6O_{10}$) is readily corroded [31]. The crystal thickness should be selected according to the time resolution desired and is typically 0.2 nm to 1 mm, cut so that the surface normal is at phase matching angle θ with the optical axis, and it may be antireflection-coated for fluorescence input and UV output, which also affords protection. The pertinent parameters are collected in Table 1. Detailed calculations are needed if the ultimate time resolution is to be achieved [32]. Caution must be exercised so that the gate intensity does not exceed the damage threshold I_d of the crystal. The lower wavelength limit for fluorescence to be upconverted is given by the optical transmission properties of the crystal, as indicated in Table 1 (for a gate at 800 nm). Regarding the upper wavelength limit, upconversion of infrared emission between 1 and 2 μm has been reported in BBO [33] and up to 5 μm in $LiIO_3$ [34].

Optics. The most demanding part of the optical setup is presented by the need to collect efficiently. The fluorescence from the sample cell and focus it onto the upconversion crystal. In order to preserve time resolution, refractive materials should be avoided and reflective optics used instead. Note that the non-linear crystal allows a maximum acceptance angle (in the extraordinary plane) for the upconversion process, and that the throughput ("étendue") E = dW (subtended solid angle of the source) × dA (illuminated area on the crystal) should be conserved for power transfer. It is important to realize that, once the maximum acceptance angle is attained, the upconversion signal cannot be further increased by only collecting more light. The spot size could be increased, but this will decrease the fluorescence intensity on the crystal and accordingly decrease the upconversion signal. An elliptical mirror allows 1:1 imaging only [24]. Two off-axis parabolic mirrors are most often used, and with different focal lengths it is possible to match the acceptance angle at the crystal, albeit at the cost of a different spot size there. When mounted correctly, as in refs. [27, 28] (and not like in Fig. 6), alignment errors partly compensate. The UV signal may be separated from the gate and pump light by a prism or a UV-transparent glass filter. Finally it is focused, typically with a lens of fused silica, onto the entrance slit of a (preferably double) monochromator.

Considerations. The fluorescence bandwidth that can be upconverted with 800-nm gate pulses is typically 200 cm^{-1} (<10 nm). This means that for every angle θ of the crystal, a kinetic trace is recorded at a frequency $\nu_U(\theta)$ in the UV, which reflects the intensity of spontaneous emission at corresponding $\nu_F(\theta)$. The situation is illustrated in Fig. 7 where a number of kinetic traces are cast across the fluorescence band in this way.

Several aspects should be considered before transient spectra can be obtained, allowing an interpretation in terms of fluorescent species. The sample concentration should be low enough so that inner filter

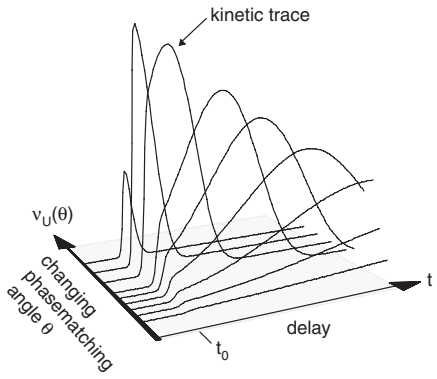

Fig. 7 The evolution of the fluorescence is sampled by kinetic traces of upconverted signal. A transient spectrum for a specific time must be reconstructed from them [35].

effects are excluded. For this purpose it is usually sufficient to adjust the pump absorption to <30%, provided that excited-state absorption is not created in the fluorescence range [36]. Second and third harmonic light from the gate will overlay the desired fluorescence signal and must be subtracted. Scattered pump light and Raman signal from the solvent give rise to a strong upconverted signal around time zero, t_0. Scattered light and Raman signal can be easily suppressed by adequate long-pass filters. The signal can also be improved if the pump light is attenuated (e.g., by using neutral density filters). The scattered signal can be used to define the instrument response function. Together with fluorescence, which can be supposed to rise instantly, it is usually possible to locate t_0 for all measured frequencies. The result should be compared with calculations of the group delay dispersion for light that travels from inside the sample to the crystal. After the traces have been aligned so that their t_0 coincide, the relative amplitudes must be scaled, for instance, by comparison with steady-state fluorescence spectra. Only then can transient spectra be constructed [15].

Improvements. Once an experimental setup is working, one may wish to improve (i) the time resolution and (ii) the accuracy by which a transient spectrum is obtained. To obtain a higher time resolution, consider that the pump and fluorescence light travel with different group velocity (GV) in the sample cell. This mismatch (GVM) limits the sample thickness, which should be calculated depending on λ_{pump} and λ_F for the desired Δt. Similarly, the major mechanism that deteriorates time resolution is GVM in the crystal between fluorescence and gate light. Thin cell windows and reflective optics must be used if all fluorescence components are to arrive on the crystal at (nearly) the same time. In practice, the fluorescence and the gate beam do not travel collinearly in the crystal but interact there at an angle $\alpha \approx 5–8°$. In this case the respective outer rays interact at different times. This so-called phase-front mismatch also spoils the time resolution [32]. Another method used to increase the time resolution is to recompress the excitation and gate pulses near to transform-limited width using sets of dispersion prisms.

In order to observe a transient fluorescence spectrum more directly (rather than by reconstruction from kinetic traces) various methods have been proposed. Already in 1983 Barbara et al. reported upconverting a 75-nm broad fluorescence spectrum by adjusting the relative convergence between the gate and fluorescence, but no details were given [37]. This very elegant approach has since remained ignored up to the more recent work by Ernsting and colleagues [38]. Gustavsson et al. built an automated setup, which may record a transient fluorescence spectrum at a desired delay time [35]. The phase matching angle is scanned, the monochromator tracks the upconverted wavelength, and the delay stage is continuously readjusted to compensate for the difference in group velocity. Haacke et al. demonstrated an original method whereby the crystal is rotated fast while the signal is dispersed by a spectrograph and integrated on a CCD [39]. This method is very practical, but one should be cautious with group velocity dispersion (GVD) when spectral coverage extending into the blue or near-UV is needed, as a temporal correction of data becomes necessary. Ernsting et al. achieved simultaneous phase matching over an 8000 cm^{-1} vis range with a fixed geometry [38]. For this purpose, they

currently use a thin (0.1 mm) BBO crystal of type II and λ_G = 1300 nm, special Schwarzschild optics, and the pulse front of the gate pulses is tilted to eliminate phase-front mismatch.

3.6 Optical Kerr gating (100 fs to 500 ps)

3.6.1 Principles

A limitation of the upconversion method is the relatively narrow spectrum range in which the emission is gated under normal circumstances (as for example, when gate pulses at 800 nm or crystal thickness >0.5 mm are used). The reason for this is the need to phase-match, as was mentioned in the preceding section. To measure the time-resolved spectra by optical gating, ideally the gating should be insensitive to the emission wavelength. This can be implemented using optical Kerr effect, as illustrated in Fig. 8.

In a manner similar to the frequency upconversion method, the ultrashort pulses are split into two beams, one is used for excitation and the other (passed to the delay line in Fig. 8) is used for the emission gating. The Kerr shutter consists of a pair of crossed polarizers (P2 and P3) and a Kerr cell. The Kerr cell can be a cuvette with CS_2, a quartz plate, or any suitable medium with large optical second-order nonlinearity [40]. Without gate pulses, the Kerr shutter blocks the sample emission. The gate pulses induce anisotropy in the Kerr cell, which changes polarization of the probed emission and let it pass the shutter. Since the anisotropy induced in a wide spectrum range (there is no resonance interaction between the emission and gate pulse), the Kerr shutter operates in a wide spectral range, limited mainly by the transmittance range of the Kerr cell and polarizers. Therefore, the detected spectrum (by a spectrograph and CCD camera) presents the time-resolved emission spectrum of the sample at the current delay time. The latter is determined by the position of the delay line.

3.6.2 Application notes

The time duration of the open Kerr shutter depends on the gate pulse duration and on the response time of the Kerr cell. CS_2 has high nonlinearity and can be used efficiently for measurements with time resolution down to 1 ps (the response time of CS_2 is 0.8 ps). For a higher time resolution (<100 fs), thin glass materials, e.g., fused silica, can be used because they have a much shorter response time [41], although the efficiency of glasses as Kerr shutters is lower than that of CS_2. A compromise solution can be utilization of benzene as Kerr medium, which has a relatively high efficiency of Kerr effect and can provide a time resolution better than 0.5 ps [42].

Certain limitations are also imposed on the polarizers P1 and P2: they must be thin enough to reduce the loss of time resolution due to GVD. Typically, sheet polarizers are preferred over prism polarizers because of their smaller thickness and bigger acceptance angle. The important parameter of the polarizer pair P2-P3 is

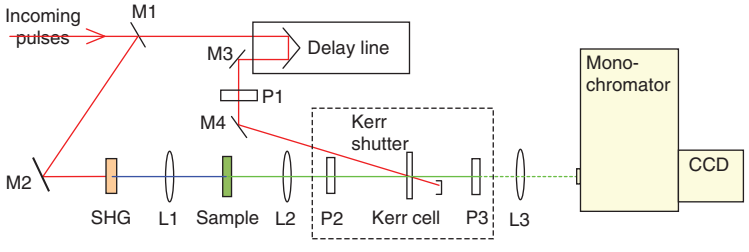

Fig. 8 Optical scheme of fluorescence time-resolved spectra measurements using optical Kerr effect. L1-L3: lenses, M1: semi-transparent mirror, M2-M4: mirrors, P1: polarization rotating plate (turns polarization of the gate pulses by 45°), P2: polarizer, P3: analyzing polarizer (must be crossed with P2), SHG: second harmonic generator.

suppression of the emission, or the ratio of emission intensities with parallel and crossed polarizers, without gate pulse, s. The residual emission passing the crossed polarizers is observed as the background spectrum and can exceed the measured signal if $s < \tau\Delta t$, where Δt is the gate pulse width and τ is the fluorescence lifetime. This means that under similar experimental conditions the sample with a shorter lifetime (τ) will produce lower background intensity and therefore can be studied more accurately than the sample with a longer lifetime. For example, if the gate pulse width is 100 fs and the fluorescence lifetime τ is 1 ns, the suppression must be much better than 10^4, which requires high-quality polarizers. This requirement can be achieved with specially designed 2-mm Glan polarizers, which allow one to achieve suppression as high as 10^6 but do not limit the time resolution [43].

The efficiency of the Kerr cell is proportional to the gate pulse power density: the higher the power, the greater Kerr shutter transmittance. Conversely, at high peak powers the two-photon excitation of the Kerr cell (or even a very low impurity contents) gives a background signal, which may hide the measured signal. This limits the choice of materials suitable for Kerr cell applications. Different Kerr cell materials have been compared in the literature [42].

The Kerr shutters operate under relatively high peak power, which cannot be obtained directly from Ti:sapphire generators. Conversely, the gated emission intensity is weak and high repetition rates are desirable for this method to overcome the dark current detection limit of the photodetectors. Therefore, a typical laser system for this method consists of a pulse generator and a regenerative amplifier operated at typically 200 kHz repetition rate.

The main advantage of the method, as compared to frequency upconversion, is the ability to measure time-resolved emission spectra simultaneously over a wide wavelength range without phase-matching considerations. On the down-side of the method is the requirement of high pulse energies for gating and a relatively high background spectrum due to two-photon excitation of the Kerr cell material and residual transmittance of the shutter, which limits application of the method to the samples with short emission lifetimes/decay times. Also, the instrument response function is usually not symmetrical, with a tail extending to negative delay times due to nuclear response of the Kerr medium.

4 Data analysis

4.1 General considerations

To establish the model for a photophysical system, time-resolved fluorescence experiments are carried out under different experimental conditions (pH, excitation wavelength λ_{ex}, emission wavelength λ_{em}, co-reactant concentration, quencher type and its concentration, temperature, etc.). The time-resolved fluorescence should be viewed as a multidimensional data surface. In single-curve analysis, the time-resolved fluorescence traces are analyzed individually, and a proposed model is tested by the consistency of the recovered parameters. In many cases the fluorescence δ-pulse response function $i(t)$ can be expressed by a sum of exponentially decaying functions (eq. 2), so that the fitting parameters comprise the decay times τ_i and their associated pre-exponential factors α_i.

This conventional approach, though adequate in many cases, fails to take full advantage of relations that may exist between the α_i and τ_i of the individual time-resolved fluorescence traces. The simultaneous or global analysis of multiple decay traces uses (and tests) those relationships by keeping some model parameters in common between various related experiments [44, 45]. This type of analysis imposes directly the model on the actual decay data. The advantages of the global analysis method are the improved model-discrimination capability and the accuracy of the parameter estimates in comparison to single-curve analysis. For instance, in the standard global analysis, the decay times τ_i can be held in common (i.e., linked) between decays collected at various emission wavelengths λ_{em}. Such a multi-exponential analysis according to eq. 2 not only provides more reliable estimates for τ_i but also for the corresponding pre-exponential factors α_i, allowing an improved determination of the decay-associated spectra (DAS) [46].

In many instances, the τ_i values will vary between related experiments and hence cannot be linked. This is, for example, the case where changing the concentration in a system forming intermolecular excimers leads to changes in τ_i. The sets of (α_i, τ_i) are the empirical descriptors of the fluorescence time evolution. It is more logical to fit directly for the more fundamental underlying parameters, which determine τ_i that is, the rate constants. By estimating directly the primary parameters of interest in a single-step analysis of the entire fluorescence decay surface, the scope of global analysis is extended. This fitting procedure is known as global compartmental analysis [46–50]. The fundamental parameters in this analysis are rate constants, species-associated spectra (SAS), translational and rotational diffusion coefficients, Förster energy-transfer distance between donor and acceptor, activation energy, enthalpy and entropy of activation, spectral parameters related to absorption and emission, etc.

The recommended strategy in fluorescence decay analysis is as follows: start with single-curve analysis and then progress, if possible, to standard global analysis in terms of (α_i, τ_i) to finish with global compartmental analysis. The first step (i.e., single-curve analysis) should not be skipped, because it allows one to weed out rogue (unacceptable) experimental decay traces and to have an idea of the number of exponential terms (compartments) needed. In some cases one can proceed directly from single-curve to global compartmental analysis (when no empirical parameters are linkable).

Finally, it should be mentioned that other approaches to global fitting are used. One method that has been successfully applied to both time-resolved absorption and emission data is the singular value decomposition [51, 52]. The 3D fluorescence surface is represented by a $m \times n$ matrix whose n columns correspond to the spectral profiles (in λ) and whose m rows correspond to the kinetic traces (in t). Singular value decomposition reduces this matrix to a set of n spectral basis functions, n singular values that corresponds to the relative contribution of each spectral basis function to the total signal, and n vectors of length m that describe how each spectral basis function contributes to the kinetic signal as a function of time [53]. The advantage is that no analytical functions are needed for the data treatment but care has to be taken to include a minimum number of spectral basis functions. In particular, the singular values can be used to make a decision on the number of intermediate states involved in the relaxation of the emissive states. The disadvantage is that spectral basis functions have no physical meaning in general and their analysis may be a complex task. For example, if the sample is a mixture of two mono-exponentially decaying fluorophores with overlapping spectra but having different lifetimes, two singular values will be essentially larger than the other, which tells that two components are needed to analyze the sample emission decay. However, the spectrum corresponding to the largest singular value will be the weighted sum of the emission spectra of the two dyes, and the second spectrum will be the difference between the spectra taken with the same weight factors. In the same situation the global fitting will provide the spectra of the dyes.

4.2 Least-squares approach in the determination of the fitting parameters

Here we assume that all possible causes of artifacts (Section 5) due to sample preparation, optics, or electronics are excluded.

The most widely used method for the analysis of data in both pulse and phase-modulation fluorescence spectroscopies is based on weighted nonlinear least-squares fitting [54]. The basic principle of this method is to minimize a quantity, which expresses the mismatch between experimental (or simulated) data and fitted function. This quantity is the reduced chi-square χ_r^2, defined as the weighted sum of the squares of the deviations of the experimental (or simulated) time-resolved fluorescence data $R(t_i)$ from the estimated ones $R_c(t_i)$:

$$\chi_r^2 = \frac{1}{\nu}\sum_{i=1}^{N}\left[\frac{R(t_i) - R_c(t_i)}{\sigma(i)}\right]^2 \tag{10}$$

where N is the total number of data points and $\sigma(i)$ is the standard deviation of the i^{th} data point, i.e., the uncertainty expected from statistical considerations (noise). ν is the number of degrees of freedom

($\nu = N - p$, where p is the number of adjustable fitting parameters). If ν is large (as is always the case in single-photon timing), the value of χ_r^2 should be close to 1.0 for a good fit. When χ_r^2 is converted to a standard normal variate Z_{χ^2} (eq. 11), the required probability can be determined from a table of standard normal probabilities. For instance, $|Z_{\chi^2}| < 1.96$ for testing at the 95 % confidence level, $|Z_{\chi^2}| < 2.58$ (99 %) and $|Z_{\chi^2}| < 3.3$ (99.9 %).

$$Z_{\chi^2} = \sqrt{\frac{\nu}{2}}(\chi_r^2 - 1) \tag{11}$$

In single-photon timing, the statistics of the collected data obey in theory the Poisson distribution. The expected deviation $\sigma(i)$ is then given by $\sqrt{R_c(t_i)}$, but often approximated by $\sqrt{R(t_i)}$ (in the Gaussian limit) so that then the expression for χ_r^2 becomes

$$\chi_r^2 = \frac{1}{\nu}\sum_{i=1}^{N}\frac{[R(t_i) - R_c(t_i)]^2}{R(t_i)} \tag{12}$$

In phase-modulation fluorometry, the curve fitting is performed in the frequency domain, i.e., directly using the variations of the phase shift ϕ and the modulation ratio M as functions of the modulation frequency. Phase data and modulation data can be analyzed separately or simultaneously (i.e., globally). In the latter case the reduced chi-squared χ_r^2 is given by

$$\chi_r^2 = \frac{1}{\nu}\left\{\sum_{i=1}^{N}\left[\frac{\phi(\omega_i) - \phi_c(\omega_i)}{\sigma_\phi(\omega_i)}\right]^2 + \sum_{i=1}^{N}\left[\frac{M(\omega_i) - M_c(\omega_i)}{\sigma_M(\omega_i)}\right]^2\right\} \tag{13}$$

where σ_ϕ and σ_M are the standard deviations for phase and modulation data, respectively, and N is the total number of frequencies. In this case, the number of data points is twice the number of frequencies, so that the number of degrees of freedom is $\nu = 2N - p$. Values of σ_ϕ and σ_M must be assigned. They are frequency dependent and, in principle, can be determined at each frequency because a large number of phase shift and modulation measurements are averaged. However, it generally turns out that when such values are used in the analysis, abnormally high values of χ_r^2 are obtained, which means that such values of the standard deviations are underestimated (because of some systematic errors). Therefore, realistic frequency-independent values are to be assigned. The important consequence is that the value of χ_r^2 is not sufficient as a criterion of good fit and that only relative values can be used in accepting or rejecting a theoretical model. As a rule of thumb, for a multi-exponential decay, when χ_r^2 decreases two-fold or more by adding an extra exponential term, then addition of this term is justified.

Data analysis in phase fluorometry requires the knowledge of the sine and cosine components of the Fourier transform of the δ-pulse response function. This is of course not a problem for the most common case of multi-exponential decays, but in some cases, the Fourier transforms may not have analytical expressions, and numerical calculations of the relevant integrals are then necessary.

In addition to the numerical goodness-of-fit criteria, it is helpful to display graphical tests for both time-resolved fluorescence methods. Visual techniques are very informative and useful for observing trends in the data. Because time is the only observable independent variable in single-photon timing experiments, it is useful to plot the differences between the experimental sample fluorescence decay, $R(t_i)$, and the fitted ones, $R_c(t_i)$. Better even is plotting the weighted residuals $W(t_i)$ defined as

$$W(t_i) = \frac{R(t_i) - R_c(t_i)}{\sigma(i)} \tag{14}$$

with $\sigma(i) = \sqrt{R(t_i)}$ for high-count SPT data, whereas for low-count SPT data $\sigma(i) = \sqrt{R_c(t_i)}$.

Such a plot can be effective in choosing the correct functional form of the fluorescence δ-pulse response function $i(t)$. There should be no discernible trend in the plot of $W(t_i)$ versus time (or channel number i); only a random scatter of points about the line $W(t_i) = 0$. The patterns of such a plot can often reveal (i) bias, i.e.,

lack of fit of the proposed model [incorrect fluorescence δ-pulse response function $i(t)$] and (ii) outliers, i.e., extremely large deviations between the experimental, $R(t_i)$, and the fitted, $R_c(t_i)$, time-resolved fluorescence data in an otherwise satisfactory fit. Outliers require careful examination to find out if the reason for their particularity can be determined.

When the number of data points is large (as is the case in single-photon timing and phase fluorometry when using a large number of modulation frequencies), the autocorrelation function of the residuals defined as

$$C(j) = \frac{\frac{1}{N-j}\prod_{i=1}^{N-j} W(t_i)\, W(t_{i+j})}{\frac{1}{N}\prod_{i=1}^{N} [W(t_i)]^2} \tag{15}$$

is also a useful graphical test of the quality of the fit. $C(j)$ expresses the correlation between the weighted residuals W in channel j and channel $i + j$.

In the case of global analyses, the statistics and the graphical tests should also be calculated for each of the traces in the multidimensional data surface.

An alternative approach, the *maximum entropy method*, based on a probability theory, has also been used in the analysis of time-resolved fluorescence, producing distributions of decay times rather than specific values bound to a given analytical model [55, 56].

Finally, it should be noted that the *maximum likelihood estimation* method has been proposed to confidently analyze single-molecule fluorescence decays with a low total number of counts [57].

4.3 Fluorescence decays with underlying distributions of decay times

The fluorescence decays are most often analyzed with a sum of exponentials (eq. 2), the number of terms being increased until a satisfactory fit is obtained, with a practical limit of four exponentials. In some cases, it is difficult to assign a physical significance to the decay times. In fact, distributions of decay times or rate constants must be anticipated to best account for the observed phenomena in various situations: fluorophores incorporated in micelles, rigid solutions, sol-gel matrices, proteins, vesicles or membranes, biological tissues; fluorophores adsorbed on surfaces, or tethered to surfaces; quenching of fluorophores in micellar solutions; energy transfer in assemblies of like or unlike fluorophores; etc. [58].

Recovery of a distribution from experimental fluorescence decay is very difficult because this is an ill-conditioned problem. In the absence of a physical model, the best approach would be, in principle, the use of methods without assumption of the distribution shape such as the *maximum entropy method* and the exponential series method [55–62]. However, these methods are extremely sensitive to data quality and truncation effects. Therefore, it is of interest to use mathematical functions whose choice is *a posteriori* validated by a good fit with a small number of floating parameters. In this regard, it was shown that two functions are very well suited to the analysis of luminescence decays with underlying distributions, the well-known stretched exponential (or Kohlrausch) function [63]

$$i(t) = \alpha \exp\left[-\left(\frac{t}{\tau}\right)^{\beta}\right] \tag{16}$$

where $0 < \beta < 1$ (β has the dimension of time), and the less-known compressed hyperbola (or Becquerel) function [64, 65].

$$i(t) = \frac{a}{(1 + ct/\tau)^{1/c}} \tag{17}$$

where $0 < c < 1$. Least-squares analysis of data by means of these functions is straightforward. Reference [66] gives an overview of models and the ability to identify models for time-resolved fluorescence with underlying distributions of rate constants.

5 Artifacts and their remedies

In this section we describe only the most important artifacts and give remedies to eliminate or correct for them. A comprehensive list of possible pitfalls in time-resolved fluorescence measurements is given elsewhere [67].

5.1 Wavelength dependence

The ratio of amplitudes of the time-resolved measurements carried out at different wavelengths in otherwise identical conditions may differ from actual intensities ratio, since the sensitivity of the photodetectors (e.g., photomultiplier tubes) and efficiencies of some optical components (e.g., monochromators) depend on the wavelength. When a comparison of intensities at different wavelengths is required, the spectrum calibration procedures have to be acquired to account for the efficiency/sensitivity properties of the optical components involved. This is usually done using a sample with known emission spectrum. For example, the corrected steady-state emission spectrum of the same sample can be used for time-resolved measurements spectrum correction.

5.2 Color effect

The explicit wavelength dependence of the time-resolved fluorescence of the sample $R(t)$, due to excitation at wavelength λ_{ex} and observed at wavelength λ_{em} [i.e., $R(\lambda_{ex}, \lambda_{em}, t)$] is given by eq. 18

$$R(\lambda_{ex}, \lambda_{em}, t) = E(\lambda_{ex}, \lambda_{em}, t) \otimes i(t) \tag{18}$$

An accurate recovery of the fluorescence parameters of $i(t)$ needs the instrument response function $E(\lambda_{ex}, \lambda_{em}, t)$ measured at λ_{em} and caused by excitation at λ_{ex}. Unfortunately, $E(\lambda_{ex}, \lambda_{em}, t)$ cannot be measured directly, because the excitation light pulse at λ_{ex} cannot normally be observed at λ_{em}. When the instrument response function is weakly wavelength dependent (e.g., when using a microchannel plate PMT), one can substitute $E(\lambda_{ex}, \lambda_{ex}, t)$ [i.e., $E(t)$ measured at λ_{ex} by recording the scattered excitation pulse profile] for $E(\lambda_{ex}, \lambda_{em}, t)$. However, many photodetectors such as common PMTs and APDs exhibit a clear wavelength dependent effect on their transit time and transit time jitter. This leads not only to a time shift between the sample fluorescence signal observed at λ_{em} and the signal from the scattering solution measured at λ_{ex}, but, more importantly, also to a different pulse shape of $E(t)$ as a function of wavelength. Such distortions are called the *color effect*. In single-photon timing experiments, if the wavelength dependence consists only of a time shift, this can be corrected simply by using a time-shift parameter or a time-shifted $E(t)$ in the curve-fitting analysis program [68]. In phase-modulation fluorometry experiments, if the wavelength dependence only results in a frequency-independent time shift, this time shift can be experimentally determined and its value can be used to correct the phase and modulation data before analysis.

In addition to a wavelength-triggered time shift there might be a dependence of the detector response upon the position of the illuminated area of the photocathode (targeting) and a temporal broadening induced by the emission monochromator.

The most efficient way to overcome these difficulties is to use a reference fluorophore instead of a scattering solution. The method requires a reference compound R, which absorbs light at the same wavelength

λ_{ex} and fluoresces at the same wavelength λ_{em} as that used for the sample. Moreover, the fluorescence δ-pulse response function of the reference compound, $i_R(t)$, should be mono-exponential

$$i_R(t) = \alpha_R e^{-t/\tau_R} \tag{19}$$

where τ_R stands for the lifetime of the reference compound and α_R denotes a scaling factor. Finally, the time-resolved fluorescence data of reference, $R_R(t)$, and sample, $R(t)$, must be recorded under identical experimental conditions (λ_{ex}, λ_{em}, optical and electronic settings) [69–75], so that $E(\lambda_{ex}, \lambda_{em}, t)$ is the same for both decays. The measured time-resolved fluorescence data of sample and reference [$R(t)$ and $R_R(t)$, respectively] are related according to

$$R(t) = R_R(t) \otimes \alpha_R^{-1}\left[i(0)\,\delta(t) + \frac{\mathrm{d}i(t)}{\mathrm{d}t} + \tau_R^{-1} i(t) \right] \tag{20}$$

where $\delta(t)$ denotes the Dirac delta function and $\frac{\mathrm{d}i(t)}{\mathrm{d}t}$ represents the time derivative of the fluorescence δ-pulse response function $i(t)$.

To correct for the photomultiplier color effect in phase-modulation fluorometry measurements, the phase shift and relative modulation are measured under identical instrumental settings for a reference fluorophore R and the sample fluorophore. The values for the phase difference $\Delta\phi$ and modulation ratio m/m_R between two fluorophores, which decay mono-exponentially, are given by [76]

$$\Delta\phi = \tan^{-1}(\omega\tau) - \tan^{-1}(\omega\tau_R) \tag{21}$$

and

$$\frac{\mathrm{m}}{\mathrm{m_R}} = \sqrt{\frac{1+\omega^2\tau_R^2}{1+\omega^2\tau^2}} \tag{22}$$

where m_R denotes the modulation of the reference.

The time shift between the decay profiles recorded for sample and reference is still possible because the light paths for sample and reference may have a slightly different length because of differences in refractive index, physical sample/reference placement, or sample/reference cuvette dimensions. These resulting time shifts can be accounted for in the data analysis.

5.3 Light scattering

Light scattering results in the appearance of a signal, which is not the emission of interest and should be diminished experimentally or accounted for during data analysis. Two main causes for the scattering are elastic scattering due to a lack of the homogeneity of the medium and inelastic scattering due to photon interactions with vibrational modes of the medium. The former is called *Rayleigh scattering* when the characteristic size of inhomogeneities is much smaller than the excitation wavelength ($d < \lambda$). The latter is called *Raman scattering* and is characterized by the wavelength shift of the scattered light with respect to the excitation light.

The intensity of Rayleigh scattering (R_{sc}) is inversely proportional to the fourth power of the wavelength ($R_{sc} \propto \lambda^{-4}$). The intensity decreases quickly with decreasing size of the inhomogeneities, e.g., size of scattering particles, because it is proportional to the sixth power of the characteristic size ($R_{sc} \propto d^6$), e.g., particle diameter. The angular dependence of the scattered intensity is given by $R_{sc} \propto (1 + \cos^2\theta)$, where θ is scattering angle, and it is the lowest at the right angle to the beam propagation direction. Therefore, right angle excitation-monitoring schemes are preferable for measurements of samples with low emission intensities.

Since the scattered light wavelength is the same as that of the excitation light, the sample emission and scattering can be filtered spectrally using optical filters (e.g., cut-off or notch filters), monochromators, or other wavelength-sensitive devices.

Raman scattering takes place when the photons interact with vibrational modes of the medium. This interaction results in a shift of the wavelength of the scattered photons. If the frequency of the vibrational mode is ν_v and the frequency of the excitation light is ν_0 (corresponding to wavelength $\lambda_0 = c/\nu_0$), the wavelength of the scattered light is $\lambda_s = (\nu_v - \nu_0)^{-1}$ (Stokes) or $\lambda_{as} = (\nu_v + \nu_0)^{-1}$ (anti-Stokes).

Non-resonance Raman scattering takes place in all transparent media, although its efficiency is very low, typically $<10^{-9}$, but it may interfere with the emission spectrum of the studied sample because it is shifted in wavelength relative to the excitation. A simple test to distinguish between fluorescence of the sample and Raman scattering in such case is to change the excitation wavelength slightly. The Raman emission spectrum should change with the excitation wavelength, whereas the fluorescence spectrum should not change (although its intensity may change).

Both Raman and Rayleigh scattering have no time evolution of their own, and follow the time profile of the excitation beam. In time-resolved emission spectroscopy, scatter is observed as a short pulse with a time profile following the instrument response function. This makes it possible to distinguish between the lasting sample emission, such as fluorescence, and scattering, when the time-resolved spectra are acquired.

In phase-modulation fluorometry, when the fitting function is a sum of exponentials, the contribution of light scattering appears as an extra component required to obtain a good fit but with an unrealistic short decay time, i.e., shorter than the shortest decay time measurable by the instrument according to its time response.

5.4 Polarization effects

The fluorescence polarization or anisotropy is an important topic and is treated in detail elsewhere [8]. While being a valuable source of information regarding the molecular properties of the emitting species and its interactions with the local environment, polarization effects may seriously distort fluorescence decays and lead to erroneous results if not properly accounted for. A response proportional to the total fluorescence intensity can be observed by using an excitation polarizer in the vertical position, and an emission polarizer set at the magic angle (54.7°) with respect to the vertical, or vice versa [1, 2].

5.5 Artifacts specific to phase methods

When zero-crossing detectors are used, artifacts appear if the intensities of light from the sample and reference cuvettes are not matched, because the detectors operate then on different gain settings and different noise characteristics. It is thus recommended to adjust the concentration of the reference cuvette for optimal matching of the intensities so that the detectors operate on near-identical gain settings and identical noise characteristics in both sample and reference channels.

Matching to operate with the same gain settings is also recommended for digital acquisition analogue-to-digital converting cards.

5.6 Artifacts specific to single-photon timing

It is important that the number of pulses arising from the detection of fluorescence photons be kept much smaller that the number of exciting pulses (<0.01–0.05 pulse per exciting pulse), so that the probability of

detecting two fluorescence pulses per exciting pulse is negligible. Otherwise, since the TAC will take into account only the first fluorescence pulse, the counting statistics will be distorted: the decay will appear shorter than it is in reality. This effect is called the pulse pile-up effect (see Section 3.1.2).

The linear time response of the TAC is most critical for obtaining accurate fluorescence decay time values. The accuracy of fluorescence decay time measurements depends critically upon the calibration of the time axis of the TAC. The response of the TAC is more linear when the time during which the TAC is in operation and unable to respond to another signal (dead time) is minimized. For this reason, it is better to collect the data in the INVERSE configuration (see Section 3.3). In this way, only a small fraction of start pulses result in stop pulses and the collection statistics are better due to longer "on" time of the TAC. Current devices allow for detection of multiple photons per excitation pulse. This avoids pile-up distortions and is beneficial in the measurement of lifetimes/decay times in the 100 ns range and above.

5.7 Artifacts specific to optical correlation methods

An important remark is that fluorescence upconversion, like any other optical correlation method (like optical Kerr gating), uses a mechanical delay stage to induce a variable time delay between the excitation and the gating pulse. A typical delay stage equipped with a retroreflector may span 2×15 cm corresponding to 1 ns, with steps of 0.1 μm, corresponding to 0.67 fs. The recorded signal gives a true measure of the fluorescence intensity decay only as far as the spatial overlap between the fluorescence and the laser gating beam in the nonlinear crystals remains unchanged when the mechanical delay stage moves. It is therefore crucial to align the optical and mechanical axes of the delay stage and to verify its linearity. Likewise, it is important that the beam passing through the delay stage has negligible divergence. These two points may be a problem for longer delays, corresponding to several hundreds of ps, and single-photon counting methods would be preferable.

5.8 Artifacts related to sample preparation

As a general rule, in fluorescence measurements the concentration should be kept sufficiently low in order to avoid inner filter effects due to re-absorption of the emitted light within the sample [1, 2]. The fluorescence produced by the re-absorption is delayed, causing an apparent increase in lifetime. Simple control measurements of the emission spectrum at different concentrations should be performed and the experiments should be done at a concentration value where the shape of the emission spectrum remains unchanged.

An obvious precaution is to check the blank (solvent, buffer, etc.) in order to detect possible contamination of the signal with light scattering and/or fluorescent impurities.

Molecular oxygen (O_2), which is ubiquitous in solutions, is primarily responsible for photobleaching via photo-oxidation, while being an efficient quencher of fluorescence. Attention should thus be paid to its effect on time-resolved fluorescence. The contribution of oxygen quenching to the decay of an excited state can be expressed by a quenching term $k_q[O_2]$ to be added to the rate of de-excitation. Under atmospheric pressure, the concentration of O_2 in common solvents is 10^{-3}–10^{-4} mol·L^{-1}. Therefore, since $k_q \approx 10^{10}$ L·mol^{-1}·s^{-1} (for a diffusion-controlled process at ambient temperature), the lifetime of a fluorophore in the presence of O_2 cannot be longer than 10^{-6}–10^{-7} s in air-saturated solutions. The longer the lifetime in the absence of O_2, the stronger its sensitivity to the presence of oxygen will be. Therefore, methods to remove oxygen from solution are required. For biological samples, an enzymatic oxygen scavenging system, comprised of a mixture of glucose oxidase and catalase, can be used to remove O_2. Otherwise, solutions must be de-aerated by bubbling N_2 (or rather argon) through the solution or, preferably, by the freeze-pump-thaw technique, which is more efficient (but also more time-consuming).

6 Lifetime standards

6.1 Nanosecond (ns) lifetimes

Fluorescence lifetime standards are needed in various scientific and material research areas. Fluorophores with known lifetimes are necessary for testing the time-resolved instruments for systematic errors, for calibrating the instrumentation for time-resolved fluorescence measurements, and for use as reference compounds to avoid the wavelength-dependent time response of PMTs (the color effect, Section 5.2). To provide the research community with reliable fluorescence lifetime standards, an international, cooperative project, which involved nine research groups active in the field of time-resolved fluorescence, was undertaken [77]. Table 2 summarizes the mean lifetimes $\overline{\tau}$ and the associated sample standard uncertainties u for 20 fluorescence lifetime standards in the solvents tested. To have an idea of the precision of the experimental lifetime data, the relative standard uncertainty (the ratio of the sample standard uncertainty u over the mean lifetime $\overline{\tau}$) was expressed as a percentage, that is, 100 $\overline{\tau}$.

6.2 Picosecond (ps) lifetimes

Contrary to the ns timescale, there are no well-established standards for fluorescence lifetimes on the ps timescale. The reasons are many, one being the fact that to record "true" ps fluorescence decays, fs time resolution is needed and such techniques are quite recent compared to the more conventional ones used for ns measurements. Moreover, the choice of standards on such a short timescale is difficult in view of the problems outlined below. From a general point of view, however, it may be important to have some reference data for calibration of new experimental setups and comparison between different techniques

Table 2 Mean lifetime $\overline{\tau}$ and sample standard uncertainty u of the fluorescence lifetime standards in fluid solution at 20 °C [77].

Compound[a]	Solvent	$\overline{\tau} \pm u$ /(ns)[b]	100 $u/\overline{\tau}$	λ_{ex} /(nm)	λ_{em} /(nm)	n[c]
Anthracene	Methanol	5.1 ± 0.3	6.1	295–360	375–442	7
	Cyclohexane	5.3 ± 0.1	2.6	295–360	375–442	7
9-Cyanoanthracene	Methanol	16 ± 1	9.3	295–360	400–480	7
	Cyclohexane	12.7 ± 0.7	5.5	295–360	400–450	4
DPA	Methanol	8.7 ± 0.5	5.6	295–360	400–475	8
	Cyclohexane	7.5 ± 0.4	5.8	295–360	400–475	7
N-methylcarbazole	Cyclohexane	14.1 ± 0.9	6.2	290–325	350–400	6
Coumarin 153	Methanol	4.3 ± 0.2	4.5	295–442	495–550	5
Erythrosin B	Water	0.089 ± 0.003	3.6	488–568	550–580	6
	Methanol	0.47 ± 0.02	4.0	488–568	550–590	6
NATA	Water	3.1 ± 0.1	3.6	295–309	330–410	7
POPOP	Cyclohexane	1.12 ± 0.04	3.6	295–360	380–450	8
PPO	Methanol	1.65 ± 0.05	2.7	295–330	340–400	8
	Cyclohexane	1.36 ± 0.04	2.6	290–325	360–450	8
Rhodamine B	Water	1.74 ± 0.02	0.9	488–575	560–630	5
	Methanol	2.5 ± 0.1	4.0	295, 488–568	550–630	8
Rubrene	Methanol	9.9 ± 0.3	3.2	300, 488,514	550–610	5
SPA	Water	31.2 ± 0.4	1.4	300–330	466–520	5
p-Terphenyl	Methanol	1.17 ± 0.08	6.5	284–315	330–380	7
	Cyclohexane	0.98 ± 0.03	3.3	290–315	330–390	7

[a]Abbreviations used: DPA: 9,10-diphenylanthracene, NATA: *N*-acetyl-L-tryptophanamide, POPOP: 1,4-bis(5-phenyloxazol-2-yl) benzene, PPO: 2,5-diphenyloxazole, SPA: *N*-(3-sulfopropyl)acridinium. All solutions are deoxygenated by repetitive freeze-pump-thaw cycles or by bubbling N_2 or Ar through the sample solutions.

[b]Average (mean) lifetime $\overline{\tau}$. The quoted errors are sample standard uncertainties $u = \sqrt{\frac{1}{n-1}\sum_{i=1}^{n}(\tau_i - \overline{\tau})^2}$. Both time and frequency domain data were used to determine $\overline{\tau}$ and u.

[c]Number of lifetime data used in the calculation of $\overline{\tau}$ and u.

and/or compounds. We therefore discuss the context and list one possible, but unofficial, reference compound. Obviously, this topic deserves much more attention in the future.

In most fs fluorescence studies, the high time resolution is not used to measure the fluorescence lifetime itself but rather to study its behavior at early times, emitted under non-relaxed, non-equilibrated conditions. This may relate to electronic and/or vibrational relaxation, solvation dynamics, and other nonradiative relaxation processes affecting the fluorescence intensity, but which are outside the scope of this text. What is important is that due to these processes the fluorescence decays may contain ultrafast transients at early times, rendering them highly non-exponential and making it very difficult to quantify them by a given lifetime. Moreover, the fluorescence decays may be strongly dependent on both the excitation and emission wavelengths. All this is obviously incompatible with the notion of a lifetime reference or standard.

Conversely, there are an increasing number of ultrafast decays being measured by fluorescence spectroscopy. By ultrafast, we refer to cases of fluorescence decaying completely within 10 ps. In order to serve as a reference, any such ultrashort-lived compound should display a single exponential fluorescence decay, implicitly meaning that processes such as conformational relaxation or electron or proton transfer are excluded. One class of molecular compounds fulfilling such severe criteria are the various metalloporphyrins which, when excited in the Soret band around 400 nm, emit a short-lived blue fluorescence from the second electronically excited state S_2. The only compound for which sufficient statistics are available is zinc tetraphenylporphyrin (ZnTPP) in ethanol solution. From five fluorescence upconversion measurements [78–82] and one optical Kerr gating [40] experiment, an average lifetime value of (2.3 ± 0.1) ps was obtained for its blue S_2 fluorescence. It has been argued [82] that ZnTPP aggregates under the conditions used in many of these experiments, but it seems to have minor influence on its fluorescence lifetime.

7 ABBREVIATIONS

APD	avalanche photodiode
CCD	charge-coupled device
CFD	constant fraction discriminator
cw	continuous wave
fs	femtosecond (10^{-15} s)
GVD	group velocity dispersion
GVM	group velocity mismatch
GW	gigawatt (10^9 W)
LED	light-emitting diode
µs	microsecond (10^{-6} s)
MCA	multichannel analyzer
ms	millisecond (10^{-3} s)
NIR	near infrared
ns	nanosecond (10^{-9} s)
OPA	optical parametric amplifier
OPO	optical parametric oscillator
PC	personal computer *or* Pockels cell
PMT	photomultiplier tube
ps	picosecond (10^{-12} s)
SH	second harmonic
SPT	single-photon timing
TAC	time-to-amplitude converter
TCSPC	time-correlated single-photon counting
TH	third harmonic
UV	ultraviolet
vis	visible

8 Membership of sponsoring bodies

Membership of the IUPAC Physical and Biophysical Chemistry Division Committee for the period 2014–2015 is as follows:

***President*:** R. Marquardt (France); ***Vice President*:** A. K. Wilson (USA); ***Secretary*:** A. Friedler (Israel); ***Past President*:** K. Yamanouchi (Japan); ***Titular Members*:** K. Bartik (Belgium); A. Goodwin (USA); A. E. Russell (UK); J. Stohner (Switzerland); Y. H. Taufiq-Yap (Malaysia); F. van Veggel (Canada); ***Associate Members*:** K. Battacharyya (India); A. G. Császár (Hungary); J. de Faria (Portugal); V. Kukushkin (Russia); Á. W. Mombrú (Uruguay); X. S. Zhao (China/Beijing); ***National Representatives*:** Md. Abu bin Hassan Susan (Bangladesh); H. R. Corti (Argentina); J. Cejka (Czech Republic); S. Hannongbua (Thailand); S. J. Kim (Korea); E. Klein (Bulgaria); M. Koper (Netherlands); M. Korenko (Slovakia); K. E. Laasonen (Sweden); J. E. G. Mdoe (Tanzania); V. Tomišić (Croatia).

Membership of the IUPAC Organic and Biomolecular Chemistry Division Committee for the period 2014–2015 is as follows:

***President*:** M. J. Garson (Australia); ***Vice President*:** M. A. Brimble (New Zealand); ***Secretary*:** A. Griesbeck (Germany); ***Past President*:** K. N. Ganesh (India); ***Titular Members*:** G. Blackburn (UK); A. Brandi (Italy); T. Carell (Germany); B. Han (China); F. Nicotra (Italy) N. E. Nifantiev (Russia); ***Associate Members*:** A. Al-Aboudi (Jordan); V. Dimitrov (Bulgaria); J. F. Honek (Canada); P. Mátyus (Hungary); A. P. Rauter (Portugal); Z. Xi (China/Beijing); ***National Representatives*:** Y.-M. Choo (Malaysia); O. M. Demchuk (Poland); M. Ludwig (Czech Republic); V. Milata (Slovakia); M. Olire Edema (Nigeria); P. M. Pihko (Finland); N. Sultana (Bangladesh); H. Vančik (Croatia); B.-J. Uang (China/Taipei); T. Vilaivan (Thailand).

Membership of the IUPAC Analytical Chemistry Division Committee for the period 2014–2015 is as follows:

***President*:** D. Hibbert (Australia); ***Vice President*:** J. Labuda (Slovakia); ***Secretary*:** Z. Mester (Canada); ***Past President*:** M. F. Camões (Portugal); ***Titular Members*:** C. Balarew (Bulgaria); Y. Chen (China/Beijing); A. Felinger (Hungary); H. Kim (Korea); M. C. Magalhães (Portugal); H. M. M. Sirén (Finland); ***Associate Members*:** R. Apak (Turkey); P. Bode (Netherlands); D. Craston (UK); Y. H. Lee (Malaysia); T. Maryutina (Russia); N. Torto (South Africa); ***National Representatives*:** L. Charles (France); O. C. Othman (Tanzania); P. DeBièvre (Belgium); M. N. Eberlin (Brazil); A. Fajgelj (Slovenia); K. Grudpan (Thailand); J. Hanif (Pakistan); D. Mandler (Israel); P. Novak (Croatia); D. G. Shaw (USA).

This document was prepared in the frame of IUPAC Project #2004-021-1-300, Reference Methods, Standards and Applications of Photoluminescence. ***Chairs*:** Fred Brouwer, Enrique San Román; ***Members*:** Ulises Acuña, Marcel Ameloot, Noël Boens, Cornelia Bohne, Paul DeRose, Jörg Enderlein, Nikolaus Ernsting, Thomas Gustavsson, Niels Harrit, Johan Hofkens, Alex E. Knight, Helge Lemmetyinen, Hiroshi Miyasaka, Ute Resch-Genger, Alan Ryder, Trevor Smith, Mark Thompson, Bernard Valeur, Hiroyuki Yoshikawa.

References

[1] B. Valeur, M. N. Berberan-Santos. *Molecular Fluorescence. Principles and Applications*, 2nd ed., Wiley-VCH, Weinheim (2012).
[2] J. Lakowicz. *Principles of Fluorescence Spectroscopy*, 3rd ed., Springer-Verlag, New York (2006).
[3] M. Sauer, J. Hofkens, J. Enderlein, *Handbook of Fluorescence Spectroscopy and Imaging. From Single Molecules to Ensembles*, Wiley-VCH, Weinheim (2011).
[4] S. E. Braslavsky. *Pure Appl. Chem.* **79**, 293 (2007).
[5] J. N. Demas. *Excited-State Lifetime Measurements*. Academic Press, New York (1983).
[6] R. B. Cundall, R. E. Dale. *Time-resolved Fluorescence Spectroscopy in Biochemistry and Biology*. NATO ASI Series A: Life Sciences, Vol. 69, Plenum Press, New York (1983).
[7] D. V. O'Connor, D. Phillips. *Time-correlated Single Photon Counting*. Academic Press, London (1984).
[8] M. Ameloot, M. vandeVen, A. U. Acuña, B. Valeur. *Pure Appl. Chem.* **85**, 589 (2013).
[9] D. M. Jameson, E. Gratton, R. D. Hall. *Appl. Spectrosc. Rev.* **20**, 55 (1984).
[10] J. R. Alcala, E. Gratton, D. M. Jameson. *Anal. Instrum.* **14**, 225 (1985).
[11] J. R. Lakowicz, G. Laczko, I. Gryczynski. *Rev. Sci. Instrum.* **57**, 2499 (1986).

[12] H. B. Manning, G. T. Kennedy, D. M. Owen, D. M. Grant, A. I. Magee, M. A. A. Neil, Y. Itoh, C. Dunsby, P. M. W. French. *J. Biophoton.* **1**, 494 (2008).
[13] J. R. Grandusky, S. R. Gibb, M. Mendrick, L. J. Schowalter. *Phys. Status Solidi C* **8**, 1528 (2011).
[14] N. Tkachenko. *Optical Spectroscopy: Methods and Instrumentations.* Elsevier, Amsterdam (2006).
[15] M. Maroncelli, G. R. Fleming. *J. Chem. Phys.* **86**, 6221 (1987).
[16] W. Becker. *Advanced Time-correlated Single Photon Counting Techniques.* Springer Series in Chemical Physics, Vol. 81, Springer, Berlin (2005).
[17] I. Eom, T. Joo, *J. Chem. Phys.* **131**, 244507 (2009).
[18] A. Morandeira, L. Engeli, E. Vauthey. *J. Phys. Chem. A* **106**, 4833 (2002).
[19] J. Shah. *IEEE J. Quant. Electron.* **24**, 276 (1988).
[20] A. Yariv. *Quantum Electronics.* John Wiley, New York (1989).
[21] Y. Stepanenko, C. Radzewicz. *Appl. Phys. Lett.* **86**, 211120 (2005).
[22] H. Mahr, M. D. Hirsch. *Optics Comm.* **13**, 96 (1975).
[23] D. Anestopoulos, M. Fakis, I. Polyzos, G. Tsigaridas, P. Persephonis, V. Giannetas. *J. Phys. Chem. B* **109**, 9476 (2005).
[24] N. E. Holt, J. T. M. Kennis, L. Dall'Osto, R. Bassi, G. R. Fleming. *Chem. Phys. Lett.* **379**, 305 (2003).
[25] D. F. Underwood, T. Kippeny, S. J. Rosenthal. *J. Phys. Chem. B* **105**, 436 (2001).
[26] N. E. Holt, J. T. M. Kennis, G. R. Fleming. *J. Phys. Chem. B* **108**, 19029 (2004).
[27] E. Atas, Z. Peng, V. D. Kleiman. *J. Phys. Chem. B* **109**, 13553 (2005).
[28] T. Pancur, N. K. Schwalb, F. Renth, F. Temps. *Chem. Phys.* **313**, 199 (2005).
[29] V. G. Dmitriev, G. G. Gurzadyan, D. N. Nikogosyan. *Handbook of Nonlinear Optical Crystals.* Springer Series in Optical Sciences, Springer, Berlin (1999).
[30] S. J. Matthews. *Laser Focus World* **39**, 49 (2003).
[31] C. Chen. *Laser Focus World* **40**, 91 (2004).
[32] H. Rhee, T. Joo. *Opt. Lett.* **30**, 96 (2005).
[33] T. Koyama, Y. Miyata, K. Asaka, H. Shinohara, Y. Saito, A. Nakamura. *Phys. Chem. Chem. Phys.* **14**, 1070 (2012).
[34] Y. Takahashi, H. Kitagawa, T. Suemoto. *Phys. Rev. B* **79**, 153103 (2009).
[35] T. Gustavsson, L. Cassara, V. Gulbinas, G. Gurzadyan, J.-C. Mialocq, S. Pommeret, M. Sorgius, P. van der Meulen. *J. Phys. Chem. A* **102**, 4229 (1998).
[36] S. A. Kovalenko, R. Schanz, T. A. Senyushkina, N. P. Ernsting. *Phys. Chem. Chem. Phys.* **4**, 703 (2002).
[37] K. Ding, S. J. Courtney, A. J. Strandjord, S. Flom, D. Friedrich, P. F. Barbara, *J. Phys. Chem.* **87**, 1184 (1983).
[38] X.-X. Zhang, C. Würth, L. Zhao, U. Resch-Genger, N. P. Ernsting, M. Sajadi. *Rev. Sci. Instrum.* **82**, 063108 (2011).
[39] S. Haacke, R. A. Taylor, I. Bar-Joseph, M. J. S. P. Brasil, M. Hartig, B. Deveau. *J. Opt. Soc. Am. B* **15**, 1410 (1998).
[40] S. Kinoshita, H. Ozawa, Y. Kanematsu, I. Tanaka, N. Sugimoto, S. Fujiwara. *Rev. Sci. Instrum.* **71**, 3317 (2000).
[41] B. Schmidt, S. Laimgruber, W. Zinth, P. Gilch. *Appl. Phys. B* **76**, 809 (2003).
[42] S. Arzhantsev, M. Maroncelli. *Appl. Spectrosc.* **59**, 206 (2005).
[43] M. Sajadi, A. L. Dobryakov, E. Garbin, N. P. Ernsting, S. A. Kovalenko. *Chem. Phys. Lett.* **489**, 44 (2010).
[44] F. J. Knorr, J. M. Harris. *Anal. Chem.* **53**, 272 (1981).
[45] J. R. Knutson, J. M. Beechem, L. Brand. *Chem. Phys. Lett.* **102**, 501 (1983).
[46] J. M. Beechem, M. Ameloot, L. Brand. *Chem. Phys. Lett.* **120**, 466 (1985).
[47] M. Ameloot, J. M. Beechem, L. Brand. *Chem. Phys. Lett.* **129**, 211 (1986).
[48] M. Ameloot, N. Boens, R. Andriessen, V. Van den Bergh, F. C. De Schryver. *J. Phys. Chem.* **95**, 2041 (1991).
[49] N. Boens, R. Andriessen, M. Ameloot, L. Van Dommelen, F. C. De Schryver, *J. Phys. Chem.* **96**, 6331 (1992).
[50] M. Ameloot, N. Boens, R. Andriessen, V. Van den Bergh, F. C. De Schryver. In: *Methods in Enzymology*, **210**, M. L. Johnson (Ed.), pp. 314–340, Academic Press, San Diego (1992).
[51] W. G. Chen, M. S. Braiman. *Photochem. Photobiol.* **54**, 905 (1991).
[52] N. P. Ernsting, S. A. Kovalenko, T. Senyushkina, J. Saam, V. Farztdinov. *J. Phys. Chem. A* **105**, 3443 (2001).
[53] J. Ervin, J. Sabelko, M. Gruebele. *J. Photochem. Photobiol. B: Biology* **54**, 1 (2000).
[54] D. F. Eaton. *Pure Appl. Chem.* **62**, 1631 (1990).
[55] A. K. Livesey, J. C. Brochon. *Biophys. J.* **52**, 693 (1987).
[56] J. C. Brochon. In: *Methods in Enzymology*, Vol. 240, M. L. Johnson, L. Brand (Eds.), pp. 262–311, Academic Press, San Diego (1994).
[57] M. Maus, M. Cotlet, J. Hofkens, T. Gensch, F. C. De Schryver, J. Schaffer, C. A. M. Seidel. *Anal. Chem.* **73**, 2078 (2001).
[58] M. N. Berberan-Santos, B. Valeur. *J. Lumin.* **126**, 263 (2007).
[59] A. Siemarczuk, B. D. Wagner, W. R. Ware. *J. Phys. Chem.* **94**, 1661 (1990).
[60] J.-C. Brochon, A. K. Livesey, J. Pouget, B. Valeur. *Chem. Phys. Lett.* **174**, 517 (1990).
[61] J. M. Shaver, L. B. McGown, *Anal. Chem.* **68**, 9 (1996).
[62] J. M. Shaver, L. B. McGown, *Anal. Chem.* **68**, 611 (1996).
[63] M. N. Berberan-Santos, E. N. Bodunov, B. Valeur. *Chem. Phys.* **315**, 171 (2005).
[64] M. N. Berberan-Santos, E. N. Bodunov, B. Valeur. *Chem. Phys.* **317**, 57 (2005).
[65] F. Menezes, A. Fedorov, C. Baleizão, B. Valeur, M. N. Berberan-Santos. *Methods Appl. Fluoresc.* **1**, 015002 (2013).

[66] N. Boens, M. Van der Auweraer. *Photochem. Photobiol. Sci.* **13**, 422 (2014).
[67] M. vandeVen, M. Ameloot, B. Valeur, N. Boens. *J. Fluoresc.* **15**, 377 (2005).
[68] Z. Bajzer, A. Zelić, F. G. Prendergast. *Biophys. J.* **69**, 1148 (1995) and refs. therein.
[69] P. Gauduchon, P. Wahl. *Biophys. Chem.* **8**, 87 (1978).
[70] R. W. Wijnaendts Van Resandt, R. H. Vogel, S. W. Provencher. *Rev. Sci. Instrum.* **53**, 1392 (1982).
[71] L. J. Libertini, E. W. Small. *Anal. Biochem.* **138**, 314 (1984).
[72] M. Zuker, A. G. Szabo, L. Bramall, D. T. Krajcarski, B. Selinger. *Rev. Sci. Instrum.* **56**, 14 (1985).
[73] M. Van den Zegel, N. Boens, D. Daems, F. C. De Schryver. *Chem. Phys.* **101**, 311 (1986).
[74] Z. S. Kolber, M. D. Barkley. *Anal. Biochem.* **152**, 6 (1986).
[75] N. Boens, M. Ameloot, I. Yamazaki, F. C. De Schryver. *Chem. Phys.* **121**, 73 (1988).
[76] R. B. Thompson, E. Gratton. *Anal. Chem.* **60**, 670 (1988).
[77] N. Boens, W. Qin, N. Basarić, J. Hofkens, M. Ameloot, J. Pouget, J. P. Lefèvre, B. Valeur, E. Gratton, M. Vandeven, N. D. Silva, Y. Engelborghs, K. Willaert, A. Sillen, G. Rumbles, D. Phillips, A. J. W. G. Visser, A. van Hoek, J. R. Lakowicz, H. Malak, I. Gryczynski, A. G. Szabo, D. T. Krajcarski, N. Tamai, A. Miura. *Anal. Chem.* **79**, 2137 (2007).
[78] G. G. Gurzadyan, T. H. Tran-Thi, T. Gustavsson. *J. Chem. Phys.* **108**, 385 (1998).
[79] N. Mataga, Y. Shibata, H. Chosrowjan, N. Yoshida, A. Osuka. *J. Phys. Chem. B* **104**, 4001 (2000).
[80] G. G. Gurzadyan, T.-H. Tran-Thi, T. Gustavsson. *Proc. SPIE-Int. Soc. Opt. Eng.* **4060**, 96 (2000).
[81] U. Tripathy, D. Kowalska, X. Liu, S. Velate, R. P. Steer. *J. Phys. Chem. A* **112**, 5824 (2008).
[82] S. Velate, X. Liu, R. P. Steer. *Chem. Phys. Lett.* **427**, 295 (2006).